INVESTIGATION OF OIL/DIESEL CONTAMINATION AND WASTE WATER SEEPAGE USING 2-D ELECTRICAL RESISTIVITY AND GROUND PENETRATION RADAR

BY

AFOLABI JAIYESIMI

19010401005

A PROJECT SUBMITTED TO THE DEPARTMENT OF GEOSCIENCES, COLLEGE OF BASIC AND APPLIED SCIENCES

IN PARTIAL FULFILMENT OF THE REQUIREMENTS FOR THE AWARD OF DEGREE OF BACHELOR OF SCIENCE IN APPLIED GEOPHYSICS

AUGUST, 2022

DECLARATION

I hereby declare that this project has been written by me and is a record of my own research work.

It has not been presented in any previous application for a higher degree of this or any other University. All citations and sources of information are clearly acknowledged by means of reference.

……..

JAIYESIMI, AFOLABI OLUFEMI

……

Date

CERTIFICATION

This is to certify that the content of this project entitled '**Investigation of Oil/Diesel Contamination and Waste Water Seepage using 2-D Electrical Resistivity and Ground Penetration Radar**' was prepared and submitted by **JAIYESIMI AFOLABI OLUFEMI** in partial fulfillment of the requirements for the degree of **BACHELOR OF SCIENCE IN APPLIED GEOPHYSICS**. The original research work was carried out by him under my supervision and is hereby accepted.

PROF. E.A. AYOLABI _____

Supervisor *(Signature and Date)*

DR. O.B. BALOGUN _____

Head of Department *(Signature and Date)*

DEDICATION

This project is dedicated to the glory of Almighty God who made this program a success. To my family for their never-ending support and love with a special thanks to my parents Otunba

Olufemi Jaiyesimi and Yeye Abimbola Jaiyesimi who continued to encourage me at every turn. Also, to my siblings Folake, Bisola and Gbale.

ACKNOWLEDGEMENTS

I am most grateful to the almighty God for making it possible for me to complete my undergraduate studies successfully. I must also acknowledge the efforts of my parents for their financial and moral support. It would not have been possible without them.

My most sincere appreciation must go to my supervisor the Vice Chancellor, Professor E.A Ayolabi for all his efforts towards the successful completion of my project and my successful undergraduate study years at the Mountain Top University. My heartfelt gratitude also goes to Mr. R.P. Akinwale, Dr. M.O. Okunubi and Mr Dayo for all their assistance towards the successful completion of this work.

For their endurance, sacrificing of their time which could have been spent with their families and their constructive criticism when necessary. I must also appreciate the enduring efforts of Dr. O.B.

Balogun the Head of Department who is always ready with a solution and word of encouragement. I would also like to mention the other members of the Department of Geosciences, Mr Alao, Dr.

A.E Jonathan and Professor Olayinka. Thank you for you all have impacted on me at some point.

Lastly, I would also like to thank all my colleagues and friends who have impacted on me during my time at the Mountain Top University.

CONTENTS

DECLARATION ii
CERTIFICATION iii
DEDICATION iv

ACKNOWLEDGEMENTS v
LIST OF TABLES viii
LIST OF FIGURES ix
ABBREVIATIONS
ABSTRACT xii
CHAPTER ONE 1
INTRODUCTION 1
1.1 Background to the study 1
1.2 Statement of Problem 2
1.3 Aim and Objective 3
1.3.1 Aim 3
1.3.2 Objectives 3
1.4 Location and Accessibility 4
CHAPTER TWO 6
LITERATURE REVIEW 6
2.1 REVIEW OF PREVIOUS WORK 6
2.2 GEOLOGICAL SETTING 11
2.2.1 Geology of Dahomey Basin 11
2.2.2 Stratigraphy of Dahomey Basin 12
2.3 BASIC THEORY 15
2.3.1 General overview: (Electrical resistivity method) 15
2.3.2 Theoretical background 16
2.3.3 Electrode configuration 21
2.3.4 Factors affecting Resistivity of subsurface material 25
2.2.5 Limitations of the electrode method 27
2.4 GROUND PENETRATING RADAR (GPR) 29
2.4.1 Basic principle of operation 29
2.4.3 Limitations of GPR 30
2.4.4 Advantages of GPR 31
CHAPTER THREE 33
METHODOLOGY 33
3.1 INTRODUCTION 33
3.2 ELECTRICAL RESISTIVITY METHOD 33
3.2.1 Data Acquisition 33
3.2.3 Data Processing 36

3.3 GROUND PENETRATING RADAR 36
3.3.1 Data Acquisition 36
3.3.4 Data processing 40
CHAPTER FOUR 41
RESULT AND DISCUSSION 41
4.1 RESULTS 41
4.2 DISCUSSION OF RESULTS 41
4.2.1 DISCUSSION OF 2D ERT RESULTS IN LOCATION 1 41
4.2.2 DISCUSSION OF 3D ERT RESULTS IN LOCATION 1 50
4.2.3 DISCUSSION OF GPR RESULTS IN LOCATION 1 54
4.2.4 DISCUSSION OF 2D ERT RESULTS IN LOCATION 2 61
4.2.5 DISCUSSION OF GPR RESULTS IN LOCATION 2 78
CHAPTER FIVE 90
CONCLUSION AND RECOMMENDATIONS 90
5.1 CONCLUSION 90
5.2 RECOMMENDATIONS 92
REFERENCES 93

LIST OF TABLES

Table 2.1 The stratigraphic charts of Benin and Western Nigeria offshore Basins 14

LIST OF FIGURES

Figure 1.1 Map showing the survey 5

Figure 2.1 Geological map of Ogun state showing the study area 11

Fig 2.2 Underground current passing into homogenous ground 20

Figure 2.3a Schematic of Wenner array 24

Figure 2.3b Schematic of Schlumberger array 24

Figure 2.3c Schematic of Dipole-Dipole array 24

Figure 2.4a parameters used for defining resistivity 26

Figure 2.4b Conduction Mechanism 26

Figure 2.5 shows the relationship between the bulk resistivity and the pore fluid resistivity 30

Figure 3.1a Set up of ABEM LS during Data acquisition on Location 1 37

Figure 3.1b Set up of ABEM LS during Data acquisition on Location 2 37

Figure 3.2a Map showing survey layout of 2D resistivity and GPR traverses at Location 1 40

Figure 3.2b Map showing survey layout of 2D resistivity and GPR traverses at Location 2 40

Figure 3.3 Set up of the MALA Ground Explorer GPR 41

Figure 4.1a: Interpreted 2D inverted ER along Traverse 1 45

Figure 4.1b: Interpreted 2D inverted ER along Traverse 1 45

Figure 4.2a: Interpreted 2D inverted ER along Traverse 2 47

Figure 4.2b: Interpreted 2D inverted ER along Traverse 2 47
Figure 4.3a: Interpreted 2D inverted Electrical Resistivity along Traverse 3 49

Figure 4.3b: Interpreted 2D inverted Electrical Resistivity along Traverse 3 49

Figure 4.4a: Interpreted 2D inverted Electrical Resistivity along Traverse 4 51

Figure 4.4b: Interpreted 2D inverted Electrical Resistivity along Traverse 4 51

Figure 4.5a and b. Interpreted 3D resistivity cube (from the 2D ERT) 53

Figure 4.6. Interpreted Dynamic slices of 3D Electrical Resistivity (from the 2D ERT) 54

Figure 4.7a and b Interpreted 3D Iso-Resistivity surfaces of resistivity signature 55

Figure 4.8 Interpreted GPR radargram along traverse 1 at Location 1 57

Figure 4.9 Interpreted GPR radargram along Traverse 2 at Location 1 58

Figure 4.10 Interpreted GPR radargram along Traverse 3 at Location 1 60

Figure 4.11 Interpreted GPR radargram along Traverse 4 at Location 1 61

Figure 4.12 3D augmented view of parallel GPR Lines in Location 1 62

Figure 4.13a. Interpreted 2D inverted resistivity section on Traverse 1 65

Figure 4.13b. Interpreted 2D inverted resistivity section on Traverse 2 65

Figure 4.14a. Interpreted 2D inverted resistivity section on Traverse 3 68

Figure 4.14b. Interpreted 2D inverted resistivity section on Traverse 4 68

Figure 4.15a. Interpreted 2D inverted resistivity section on Traverse 5a 71

Figure 4.15b. Interpreted 2D inverted resistivity section on Traverse 5b 71

Figure 4.16a. Interpreted 2D inverted resistivity section on Line 6a 74

Figure 4.16b. Interpreted 2D inverted resistivity section on Line 6b 74

Figure 4.17a. Interpreted 2D inverted resistivity section on Line 7a 77

Figure 4.17b. Interpreted 2D inverted resistivity section on Line 7b 77

Figure 4.18. Interpreted (elevation corrected) 2D inverted resistivity section on Line 8 79

Figure 4.19 Interpreted GPR radargram along Traverse 1 at Location 2 81

Figure 4.20 Interpreted GPR radargram along Traverse 2 at Location 2 82

Figure 4.21 Interpreted GPR radargram along traverse 3 at Location 2 84

Figure 4.22 Interpreted GPR radargram along traverse 4 at Location 2 85

Figure 4.23 Interpreted GPR radargram along traverse 5 at Location 2 87

Figure 4.24 Interpreted GPR radargram along traverse 6 at Location 2 88

Figure 4.25 Interpreted GPR radargram along traverse 7 at Location 2 90

Figure 4.26 Interpreted GPR radargram along traverse 8 middle line at Location 2 91

ABSTRACT

Geophysical surveys were carried out at two separate locations within the Mountain Top University Main campus located inside MFM Prayer City, Ibafo, Ogun State, Nigeria in order to investigate an oil/diesel and waste water contamination sites using 2D Electrical Resistivity Tomography and Ground Penetrating Radar. The objectives of the study are to delineate the extent of the contamination at both sites while also determining the potential effects the contamination could have on its surroundings and other bio life existing within its proximity.

At the first location, four 2D ERT traverse lines were established using 0.2 m and 0.5 m electrode spacing with the aim of providing a high-resolution image of the subsurface. At the second location, eleven 2D ERT lines were established on eight traverses with 0.1m electrode spacing (two 2D ERT lines were overlapped on lines 5 to 7). Similarly, four GPR traverse lines were established using 450 MHz antenna in location 1. At the second location, eight GPR traverses were surveyed with a 450 MHz antenna and the eighth traverse is perpendicular to others in the North to South direction along the slope of the investigated area.

In the first location, the results of the electrical resistivity have shown that the waste water seepage is represented by relatively low electrical resistivity range 1 to 20 Ωm and have penetrated a depth range of 2.7 to 3.5 m. The increase water saturation in the seepage polluted region has resulted in increased amplitude in the radargram and has helped in delineating the seepage region. Additional pipe other than the visually observed pipe in the investigated area has been mapped with the GPR method which could be another source of seepage. At the second location, the oil/diesel waste is characterised by relatively high electrical resistivity range of 120 to 13,161 Ωm and have penetrated a depth range of 0.2 to 0.85 m while the oil/diesel waste has resulted in amplitude attenuation on the GPR method.

It can be concluded that the waste water contamination to the ground surface is a result of more than one pipe leaking at different positions besides the possibility of the underground tank leakage. There is no evidence from the result to support that the contamination has invaded any potential groundwater source although its effects on the biosphere are not immiscible. In location 2, the trend of flow of the oil/diesel waste effected by the topographical changes of the site and is observed to have spread laterally beyond its point of entry onto the site. The result has provided localized spots of possible oil/diesel waste accumulation that can be used for mitigation measures.

CHAPTER ONE

INTRODUCTION

1.1 Background to the study

Soil has many varying functions aside from providing the primary form for which plant exist and reproduce it also has the function of separating and absorbing while also restricting the movement of toxic material further which could harm other components of the biosphere (Wyszkowski et al., 2020). Diesel, a petroleum secondary product is a fuel high in demand globally because of its ability to provide high amounts of energy during use. Soil contamination caused by diesel has noteworthy impact on the soils by creating a shortage of nutrients vital to the soil like nitrogen and phosphorus (Mitter et al., 2021) Aside from affecting soil properties diesel contamination will affect the water retaining ability of the soil and its oxygen holding capacity. Major areas of contamination are industrial facilities and areas where oil is usually extracted, processed and stored (Adam et al., 2002). Petroleum material serve to be a source of insecurity to humans and animals by putting at risk the safety of drinking water when it percolates into the ground and ground water resources (Wang et al., 2008) Some of the petroleum substance materials will be absorbed into the soil or higher up to the plants where it will build up. Most importantly petroleum has the ability to vaporize into the air from both soils and surface waters which in turn can produce sever effects on the breathing systems of animals and humans (Cheng and Nathanial, 2009) in particular causing mutagens and malignant agents in humans.

Groundwater pollution also occur when unsuited materials caused by human undertaking percolate water bodies underground (Ademila, 2016). A Septic tank system also known as ‘’on-site wastewater treatment system is created solely for the purpose of human excreta management. The system is made of two major parts septic tank and field lines or soil absorption field. The

tank is water tight constructed of either fiberglass or concrete consisting an inlet and outlet pipe. Groundwater contamination is most probable in areas like suburban where septic tanks are placed in close proximity to each other and also where the cover layers of soil is very thin. Drainage and human excreta from these septic tanks will be able to find their way to the surface and into the groundwater bodies causing pollution of the bodies with various chemicals and pollutants such as phosphorus, nitrate, chloride, sulphate, household chemicals, oils detergents, bacteria, viruses and other pollutants which can cause problems for the people within the environment and harming the environment in the process.

Due to the dependency on groundwater for consumption, agricultural use and other production scopes it has become paramount that both surface water and groundwater are feasible for use and groundwater materials are not being stretched all over the world because of contamination (Ademila,2016). As a result, there needs to be good standard of groundwater quality to make better the lives of people living in the environment.

1.2 Statement of Problem

Mountain Top University (MTU) rely heavily on the use of diesel generators which are used to power its several buildings which include its different colleges, staff quarters, student hostels and cafeteria during the day when power outages occur as a result of power not being supplied from the national grid. The result of constant use over time has led to the accumulation of an oil/diesel waste which is visible on the surface in front of one of the generator houses in front of CBAS (College of Basics and Applied Sciences). This waste has contaminated the ground and soil and likely to have percolated into the water table with a flowing stream close by. This oil/diesel contamination will also affect plants and other living organism's part of the biosphere.

At the Mountain Top University (MTU) main campus behind one of the female hostels exists a waste water seepage flowing onto the surface. This seepage is very evident on entrance into the site while the contamination covering laterally extensive area beyond the point of exposure. This seepage will harm plant life in the area and other organisms. The contaminants have percolated into the ground and to a considerable depth potentially seeping into any possible groundwater aquifer and contaminating the soil. There is therefore the need to carry out this investigation in order to determine the extent of the contamination at both sites.

1.3 Aim and Objective

1.3.1 Aim

The aim of this research is to investigate the oil/diesel waste at the College of Basic and Applied Sciences (CBAS) generator house and the waste water seepage at one of the hostels in MTU Campus in order to determine the extent of the pollution using 2D electrical resistivity and Ground penetrating radar method.

1.3.2 Objectives

The objectives of the study are to:

i. Characterize the subsurface based on its electrical resistivity properties and dielectric contrast
ii. Identify the anomalous response that can be associated to oil/diesel and septic tank seepage in electrical resistivity and GPR iii. Delineate the depth extent of region(s) that have been contaminated by oil/diesel waste and by the waste water seepage iv. Providing imminent representation that can be used in mitigating the effect of the oil/diesel waste and waste water seepage in future works.

1.4 Location and Accessibility

Two locations are investigated within the MTU main campus. The first location is the female hostel where a seepage of wastewater is observed while the second location is at the generator house where effluents of oil/diesel are observed. The locations fall within the geographic coordinate of latitudes N6° 43’ 52.5” to N6° 43’ 45.6” and longitudes E 3° 23’ 31.7” to E3° 24’ 44.8” (WGS, 1984). Mountain Top University is located within MFM Prayer City along Lagos Ibadan Expressway, Ogun state, Nigeria. Mountain Top University can be accessed via the LagosIbadan Expressway. Figure 1.1 displays a map indicating the location of the study area.

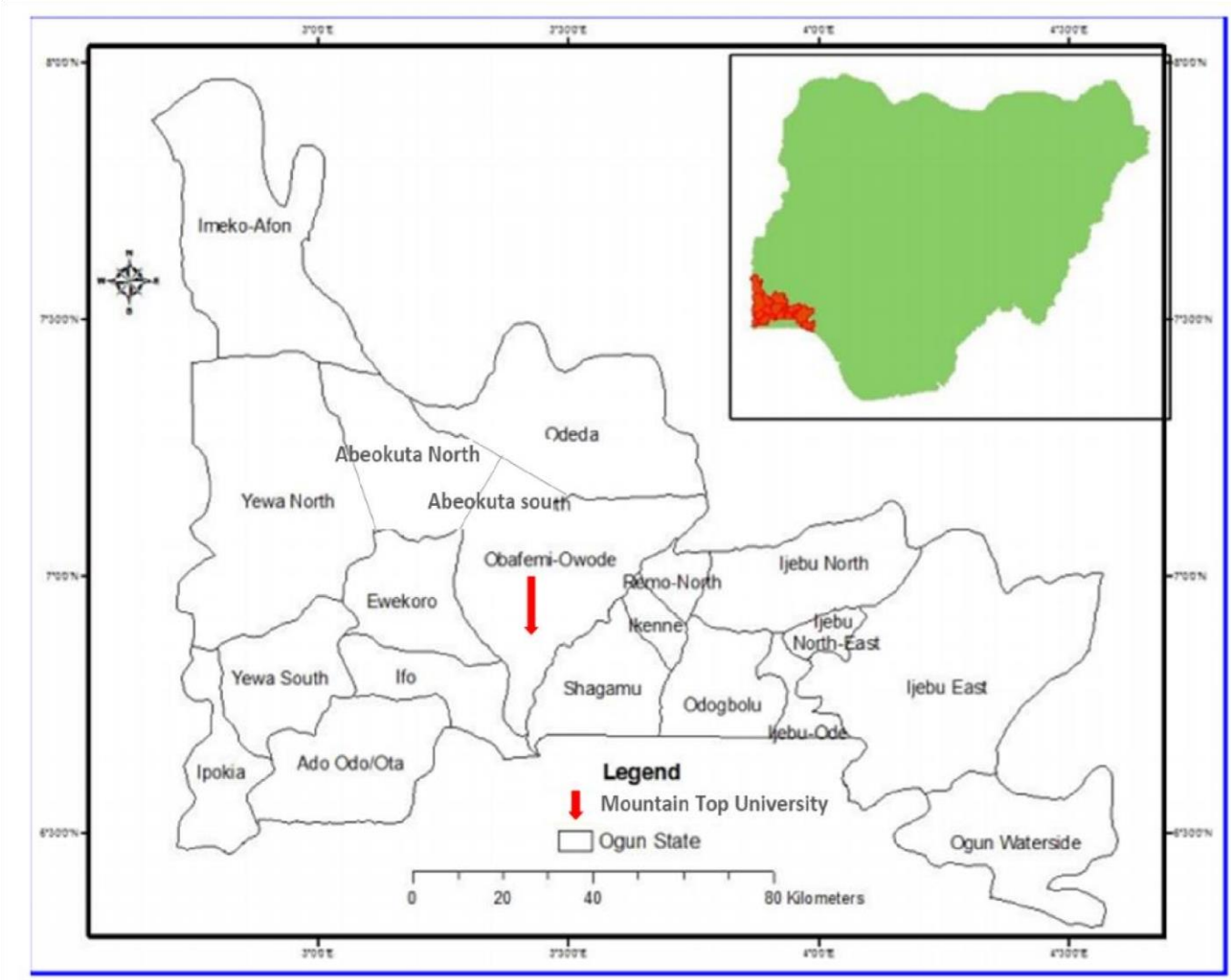

Figure 1.1 Map showing the survey area (inset map of Nigeria showing location of Ogun State within Nigeria). Modified after Oyedepo *et al*., 2013.

CHAPTER TWO
LITERATURE REVIEW

2.1 REVIEW OF PREVIOUS WORK

Previous works carried out by other researchers have been documented. A review of these works is presented below.

Daniels et al. (1995) carried out an investigation using Ground penetrating radar (GPR) for near surface pollution delineation in northern Indiana. The surveyed showed how GPR can be used to determine hydrocarbon in the vadose zone. A controlled survey was carried out with the results showing distinct GPR anomalies over vessels of diesel contamination and vessels holding multitude sand material completely filled with diesel.

At a gasoline spill site GPR data was acquired over the seasons of the years (summer, fall and winter). The data was related and showed the various layers and lenses in the vadose zone which collected water during the wet seasons and lost water during the dryer seasons. GPR data acquired during the winter across partly ice-covered grounds displayed measurements which reacted more to the presence of gasoline in contrast to measurements acquired during the dryer seasons. The comparative propagation of GPR signal on the near surface zones taken during the winter months across partly ice-covered grounds produced data from which determining the water table was possible which could not be recognised from the two further data set. Four key points can be concluded after comparing the four data sets. (1) GPR data set quality and repeatability acquired across clean sand is dependent on the water content present in the unsaturated zone above the water table. (2) GPR responses from sedimentary features are notable from responses due to percolating groundwater. (3) GPR data set acquired during the dryer

months particular August show a void of responses above the gasoline contamination which shows that water in the unsaturated zones could have been replaced by either liquid gasoline or gasoline vapours. (4) This survey serves to show the determining influence of Ground penetrating radar.

Porsani et al, (2002) carried out a GPR investigation in Sao Paulo Brazil in order to map an area contaminated with solid remnants at a refuse dump site. Eight (8) GPR lines were observed with antennas of 50 MHz and 1000 MHz. Six (6) of the lines were observed in the waste site while the reaming two additional lines were observed outside of the site. Four Vertical Electrical Sounding (VES) points were surveyed to study the depth of the contamination and delineate the base of the landfill site. Two VES points were surveyed outside the site with the aim of determining the point where the ground water table starts and observing the geoelectric stratigraphy of the background.

Interpretated results obtained from the GPR profiles indicated the top of the contamination also showing the direction of the travelling contamination to be moving laterally outside the bounds of the waste site. This was detected from a profile located 20m away from the boundary of the site. The signature response produced seemed as a discontinuous reflection which is an indication of a shallow ground water table. This discontinuity is associated with a shadow zone which is indicative of contaminant conductive deposit. The contamination did not reach a sugarcane plantation located 100m away from the boundary of the site. In areas where no contamination exist a ground water table was identified at a 10m depth and the reflective response associated with was both continuous and strong. The GPR signal was able to penetrate deep into the subsurface producing signatures at a depth of about 14m which was recognized as the boundary between two contrasting formations. The strong reflections produced as a result of the contrast in

formations was due to the presence of gravel characterized by ferruginous concretes. Interpretation of the VES profiles identified contamination zones with its bottom being range of 11m to 15m. The results of the VES surveys carried out outside the site identified no contamination in the area also identifying the top of the water table and the boundary between two contrasting formations. The results obtained from the GPR and VES were in contract with both integrations being reinforced by local geology along with evidence derived from several boreholes of about 17m depth. The base of the site is about

14.5m.

Amidu and Olayinka (2006) carried out an integrated survey in Ibadan, Southwestern Nigeria involving electrical resistivity imaging and geochemical analysis in dealing with the effects sewage disposal systems has on its surroundings. Underlaying the study area is quartzites and quartz schists with its weathered profile being sandy and silty clay with gravel. Twenty – two electrical resistivity profiles were established during this survey using the Wenner array having electrode spacing of in range 1 to 8m. The electrical resistivity data were investigated with inversion making use of a rapid least-square technique and the creation of iso- apparent resistivity contour maps. Four pits were excavated with two of them being located on areas with low resistivity and the other two situated on areas of high resistivity. The depth of each pit was 2m with soils samples being taken at depth intervals of 0.5m, 1.0m,1.5m and 2.0m. Each sample was carefully studied for conductivity values and for minerals Pb, Fe, Cu, Cr and nitrates. The results obtained from the surveys showed low resistive values near the septic tank with higher values being observed further away from the septic tank. These results are consistent with the electrical conductivity values obtained from the soil samples. Statistical studies of electrical conductivity

contrasted to distance from the septic tank produced a negative correlation between range -0.92and -0.52 which shows an inversely proportional relationship between the two parameters. Chemical analysis also produced similarly consistent results. From both the soil samples studies and geophysical results it is evident that the septic tank is affecting the environment. The results also signify that pollution mapping is possible in a basement complex

Metwaly et al, (2012) carried out an investigation at Gulf of Surez, Egypt to map subsurface oil contamination flow at an oil producing field. About the oil spill on the waste dump site four 2D electrical resistivity tomography survey lines were carried out. Prior to the survey being carried out theoretical soil resistivity reactions against fluid resistivity for various cation interactions has been considered. A physical model displaying the flow of the oil over the groundwater of flooded fluvial sediments was presented. It was suggested that the oil has high resistive values with increasing conductive values being observed farther away from the source of the spillage due to the effects of biodegrading. This variation in contamination dispersal and range of resistivity values were taken into account during the interpretation of the data set. The interpretation of the 2D resistivity profiles indicate that oil plumes have collected in the direction opposite to the sea while also providing low signatures from the profiles parallel to the shore line.

Ademila and Omowumi (2016) carried out an integrated investigation to determine water quality degradation through various pollutants due to septic tank effluent using integrated electrical resistivity imaging, physiochemical and microbiological analyses of various water samples. Ten wells and three boreholes were excavated around residential areas encircled with multiple septic tanks by standard field and laboratory procedures. Interepretation of results obtained from nine 2D profiles within the study area with Wenner configuration and electrode spacing of 2 to 12m produced lowly resistive anomalous zones with values less than 20 Ωm indicating possible septic

plume build-up. In the Northern and Southern areas of the study area the contamination build up is more projecting to a depth of about 10 m. The groundwater flow direction gives strong indications of the water in the wells flowing in a direction towards the contamination plume.

Physiochemical studies of the groundwater samples suggest it to be within drinking specifications.

Studied water samples from wells 6 and 7 show increased levels of concentration this being a result of their proximity to the septic tank system. Microbiological studies of the water samples produce extreme number of microbes present which is an indication of contamination of the groundwater resulting from the waste flow of the septic tank. In recommendation of the study water treatment and regular monitoring of groundwater sources should be suggested as well as the placing of septic tanks at considerable distance from groundwater sources.

Amin et al, (2018) carried out an investigation using GPR to map a petroleum pipeline leakage and its impact on the surrounding soils, determining the physical properties of adulterated soil and find out the electromagnetic wave signature for petroleum spill in sand. A model of the leakage was created and introduced. The data set was acquired at an hourly interval for a duration of sixteen hours in an attempt to study the petroleum leakage diffusing. The data set was processed using Reflex 2DQuick. The method used during this survey is the Finite Difference Time Domain (FTTD) which was used to create the imitation of the petroleum leak diffusion by imitating travelling electromagnetic waves through various materials. The results obtained from this study indicate an increase in dielectric constant of the sand from 3 to 5.3 in the presence of petroleum. This is due to the aptitude to store electrical energy. Data was acquired for a total duration of 16 hours every hour. Reflex 2DQuick software was used to process the raw GPR data. The outcome for the study shows the dielectric constant of the soil increase from 3 to 5.3 in the presence of petroleum. This is a result of the storability of sand. The results obtained from the GPR signal modelling Through GPR signal modelling demonstrated that the petroleum inhibited the signal attenuation being transferred from the antenna.

2.2 GEOLOGICAL SETTING

2.2.1 Geology of Dahomey Basin

The geology of Ogun state (Fig 2.1) consists of both sedimentary rocks and basement complex rocks. The sedimentary rocks are within the Eastern Dahomey Basin, the oldest being the

Abeokuta Formation. This formation is overlaid by the Ewekoro Formation and both Oshosun and Ilaro Formation consequently. All these formations are overlain by the Benin Formation or the Coastal Plain Sands (Badmus and Olatinsu, 2009).

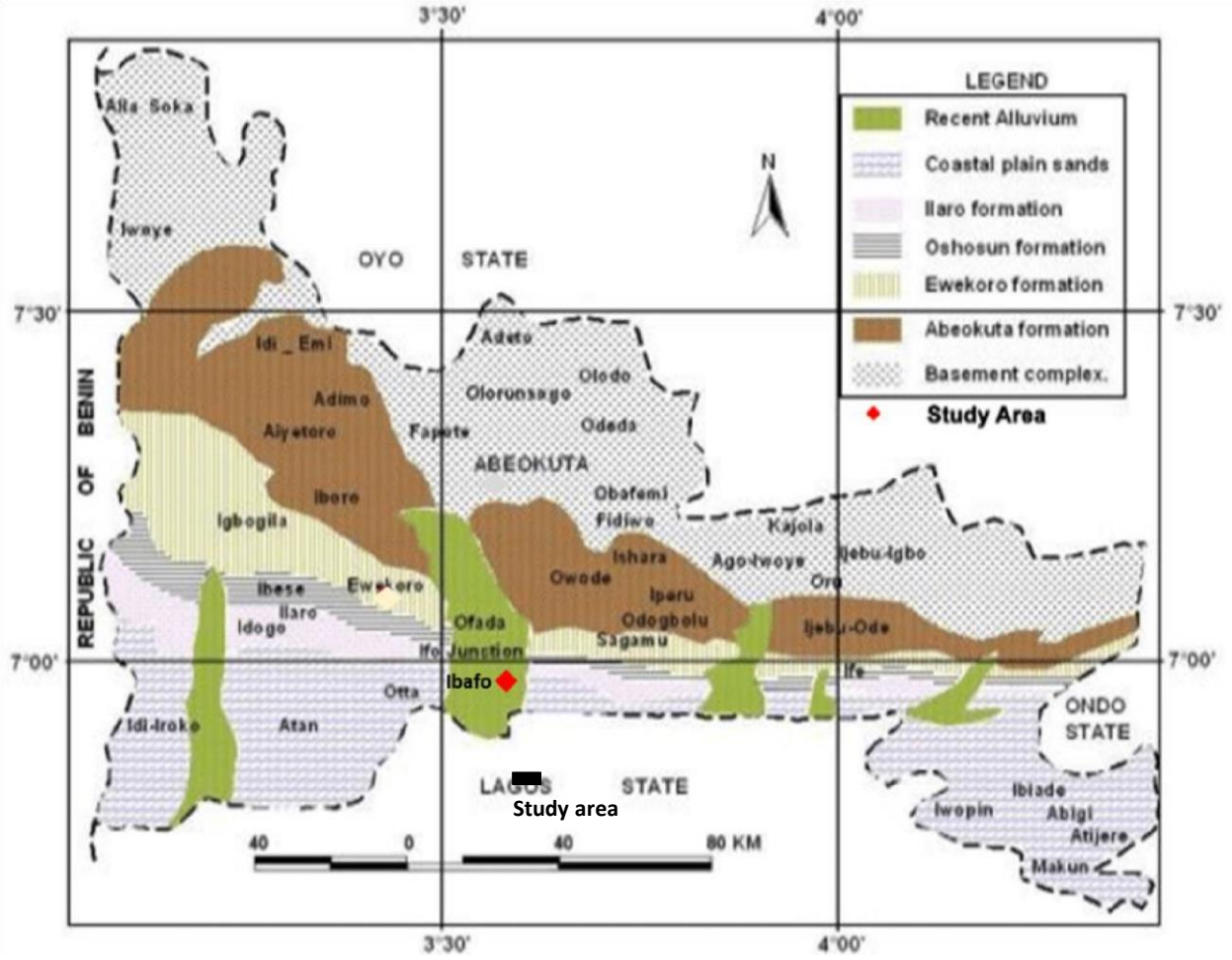

Figure 2.1 Geological map of Ogun state showing the study area within the Eastern Dahomey Basin (Adapted from Akinyemi, Olukayode, 2015

2.2.2 Stratigraphy of Dahomey Basin

There are four (4) countries to which the Dahomey Basin is found. These are named Ghana, Togo, the Republic of Benin and Federal Republic of Nigeria. The Dahomey Basin is a sedimentary basin which can be found on the Gulf of Guinea oil province. Rocks of both cretaceous tertiary age group are exposed and are seen along main roads and quarries in the Eastern part of the Basin. The Eastern section of the basin that is located in Nigeria is found in the Southwestern parts of Nigeria with the basin running through Lagos, Ogun and Ondo states respectively. This basin is present in both the onshore and offshore. The exposed cretaceous and tertiary rocks areas are found on the onshore. It has been established by authors in previous works that two structural elements are presents that make up the Benin basin and the Katipunan structures. Three (3) geoblocks have been recognized:

(i) The onshore geoblock which consists of Bodashe, IIeppa-Ojo geoblock

(ii) The Okitipupa structure made up of Union-Gbekebo geoblock (iii) The offshore geoblock.

It has been established that these geoblocks have undergone the three main stages of basin evolution. The three stages are the initial graben (pre-rift), prolonged transitional stage and open marine drift phase. Early works on the basin revealed both cretaceous and tertiary sediments. Also, three chronostratigraphic units were revelled being pre- lower Cretaceous folded sequence, cretaceous sequence and lastly tertiary sequences. The cretaceous stratigraphy is revealed to be of the Abeokuta Group which comprises three sub-formations units which are Ise Formation, Afowo

Formation and Araromi Formation. The Ise Formation is to be found over the basement complex with coarse conglomeratic sediments as its main constituents.

The Afowo Formation is made up mostly of sands from either transitional or marine terrains with sandstone which have changing and thick shales and siltstones which are highly interstratified. The Araromi, the youngest of the beds can be found on the top most of the layers which consists of shales and siltstones with interstratified limestones and sands. The tertiary stratigraphy contains sediments of Ewekoro, Akinbo, Oshosun, Ilaro and Benin. Ewekoro is made up of highly fossilized limestone of good bed setting. The Akinbo Formation as well as Ososhun Formation consists of limp shale of grey and black colours. The fringes between the Ewekoro and Akinbo Formations is a layer of glauconite beds and phosphatic beds. The remaining two formations Ilaro and Benin consists of coarse sandy estuarine, deltaic and continental beds (Olabode and Mohammed, 2016)

Table 2.1 The Stratigraphic Charts of Benin and Western Nigeria Offshore Basins

AGE		FORMATIONS			
		WESTERN NIGERIA BASIN			OFFSHORE BENIN BASIN
		Onshore Omatsola &Adegoke (1981)		Offshore	
QUART.	PLEISTOCENE-RECENT	BENIN Fm.		BENIN Fm.	BENIN/IJEBU Fm.
TERTIARY	EOCENE-PLIOCENE	ILARO Fm.			
		OSHOSUN Fm.			AFOWO Fm.
				ILARO Fm.	
				OSHOSUN Fm.	OSHOSUN Fm.
		AKINBO Fm.			
				AKINBO Fm.	IMO Fm.
	PALEOCENE	EWEKORO Fm.		EWEKORO Fm.	
CRETACEOUS	CAMPANIAN-MAASTRICHTIAN	ABEOKUTA GROUP	ARAROMI Fm.	NKPORO Fm.	ARAROMI Fm.
					AWGU Fm.
	TURONIAN-CONIACIAN		AFOWO Fm.	AWGU Fm.	ABEOKUTA Fm.
				AFOWO Fm. (ABEOKUTA Fm.)	
	NEOCOMIAN-CENOMAIAN		ISE Fm.		
				ISE Fm.	ALBIAN SST.
					ISE Fm.

2.3 BASIC THEORY

2.3.1 General overview: (Electrical resistivity method)

Electrical resistivity method can be classified as an active method in geophysics. It makes use of an artificial source with the aid of electrodes introducing current into the ground. This method measures potential difference across two electrodes around a current bearing area. Apparent resistivity can be calculated by making use of the potential difference measured across the electrodes. Current electrodes are electrodes which introduce current into the ground while potential electrodes are electrodes to which potential difference are measured across. Electrical method makes use of either direct current into the ground or low frequency alternating current (Brooke and Keary, 1984) In cases involving a homogenous ground current penetration into the ground increases as electrode spacing is increased. The spacing between the current and electrode is selected with a desired depth of investigation in mind. This may place real restrictions on achievable depths of investigations when carrying out some surveys due to the incapability to lay long lengths of cables or to generate sufficient power. The two main types of measures employed during electrical resistivity surveys are Vertical electrical sounding (VES) and Constant separation traversing (CST). VES is deployed in surveys involving horizontal or near surface horizontal investigations. Both the current and electrode are kept at a constant spacing with the spread continuing lengthwise at a static point. This technique is used to determine overburden thickness. CST is a technique used to investigate lateral resistivity variation in the subsurface. The current and potential electrodes are kept constant while continuing along the traverse. This technique is used to determine the position of faults or shear zones and identify localized bodies producing anomalous conductivity responses.

2.3.2 Theoretical background

Electrical method makes use of direct currents or low frequency alternating currents to investigate and determine the electrical properties of the subsurface. Nonconformities of patterns expected from potential difference in a homogenous ground provides evidence of the form and electrical properties of the subsurface.

The resistivity of a material is quantifiable as its resistance in ohms between the opposite faces of a unit cube of the material. A conducting cylinder of resistance δR length δL and cross-sectional area δA the resistivity is defined as ρ and is given by

$$\rho = \frac{\delta R\ \delta A}{\delta L} \tag{2.0}$$

Resistivity is measured in ohm-meter with its reciprocal conductivity being measured in Siemens (S) per meter. Some minerals are able to conduct electricity through electrons. Most rock forming minerals are insulators with electricity passing through via the ions in pore water. This leads to porosity being very important and a main regulator of rock resistivity with a general trend of resistivity increasing as porosity decreases. This does exclude crystalline rocks who have negatable to zero intergranular porosity but are conductive due to the presence of cracks and fissures. It is expected that there is overlay between different rock types making it problematic in recognising rocks only on their resistivity. Equation (1.0) denotes to electronic conduction but is also used to describe effective resistivity of a rock which is the resistivity of the rock and its pore water. Effective resistivity is also represented in relation to resistivity and volume of the present pore water according to archies formula.

$$\rho = a\Phi^{-b} f^{-c} \rho_w \tag{2.1}$$

In this equation **Φ** is the porosity, f is the fraction of pores that contains water of resistivity ρ_w with a,b and c being empirical formulas.

When current I passes through a cylinder a potential drop -δV occurs. Ohms law recounts current, potential difference and resistance as δV = δRI. Continuing from equation (1.0) δR = ρδL/Δa.

After substitution we get $\frac{\delta V}{\delta L} = -\frac{\rho I}{\delta VA} = -\rho i$ (2.2)

Where $\frac{\delta V}{\delta L}$ is the potential gradient through the material measured in Volt m^{-1} with i being the current density measured Am^{-2}. The current density in any direction in a material is usually indicated by the negative partial derivatives of the potential in that direction divided by the resistivity. When we look at a single current electrode on the surface of a medium which has unchanging resistivity ρ. Current moves outward away from electrodes that its dispersal is even over the centre of spheres source. At distance r the away from the electrode the shells surface area is $2\pi r^2$, current density then becomes

$$i = \frac{I}{2\pi r^2} \quad (2.3)$$

The potential gradient related to the current density then becomes

$$\frac{\delta V}{\delta r} = -\rho i = -\frac{\rho I}{2\pi r^2} \quad (2.4)$$

$$V_r = \int \frac{\rho I \partial r}{2\pi r^2} = \frac{\rho I}{2\pi r} \quad (2.5)$$

Equation (6.0) permits potential at any point below the surface to be calculated in a homogenous half space. The hemispheres shells contain constant voltages and are labelled equipotential surfaces. When in view of cases where the current sink is at a limited distance from the source its

potential V_c at an interior electrode C is the totality of the potential contributions V_a and V_b resulting from the current source at A and sink B.

$$V_C = V_A + V_B \tag{2.6}$$

Continuing from equation (6.0)

$$V_C = \frac{\rho I}{2\pi}\left(\frac{1}{r_A} - \frac{1}{r_B}\right)$$

(2.7) Correspondingly

$$V_D = \frac{\rho I}{2\pi}\left(\frac{1}{R_A} - \frac{1}{R_B}\right) \tag{2.8}$$

It is difficult to measure absolute potentials so potential difference is measure instead ΔV between corresponding electrodes C and D

$$\Delta V = V_C - V_D = \frac{\rho I}{2\pi}\left\{\left(\frac{1}{r_A} - \frac{1}{r_B}\right) - \left(\frac{1}{R_A} - \frac{1}{R_B}\right)\right\}$$

(2.9)

Therefore

$$\rho = \frac{2\pi\Delta V}{I\left\{\left(\frac{1}{r_A} - \frac{1}{r_B}\right) - \left(\frac{1}{R_A} - \frac{1}{R_{Bs}}\right)\right\}} \tag{2.10}$$

In the case of a uniform ground the resistivity calculated from equation (11.0) should be continuous and independent of the electrode space and surface position. When the subsurface is inhomogeneous electrode positioning will affect resistivity values producing apparent resistivity

ρ_a as a result and will represent the form of inhomogeneity in the subsurface.

Equation (2.10) is used for calculating apparent resistivity for all electrode configurations. Several electrode configurations have been considered with many being employed for particular investigations only two are frequently operated. In the Wenner electrode set up both current and potential are kept at equivalent distance a from each other. This configuration is simpler. When this value is added into equation (2.10) we simply get

$$\rho_{a} = 2\pi a \frac{\Delta V}{I} \quad (2.11)$$

When a VES survey is being carried out a is progressively enlarged around a fixed point while in CST the entire spread is moved with a staying constant. VES can be greatly improved and made more effectual by using a multicore cable allowing the addition of more electrodes. The rate of VES survey can be increased by the interchanging of various sets of four electrodes. The benefit of using such an arrangement is the quantity of ground resistance measured at any two electrode array positions decreases substantially the effects of lateral surface resistivity variation. The rigorous nature of the Wenner configuration where all four electrodes need to be moved consequently after completing positive readings is overawed somewhat by the Schlumberger configuration. When using this configuration its two inside potential electrodes are given a spacing of 2*l* which in comparison to the external current electrode spacing 2L is a small fraction. When carrying out a CST survey using the Schlumberger configuration numerous adjacent arrangements can be accomplished without the need of the electrodes moving. When working with VES and the Schlumberger configuration the potential electrodes are kept constant with the current electrodes being separated equally about the centre of the spread. When values of L are large it may become necessary to increase I in order to ensure a reasonable value for the potential difference is obtainable.

Schlumberger configuration

$$\rho_{a} = \frac{\pi (L^2 - X^2)\Delta V}{2l(L^2 + X^2)\ I} \quad (2.12)$$

X is defined as the midpoint of both current electrodes and potential electrodes. When used proportionally x = 0, therefore

$$\rho_{a} = \frac{\pi L^2 \Delta V}{2l\ \ I} \quad (2.13)$$

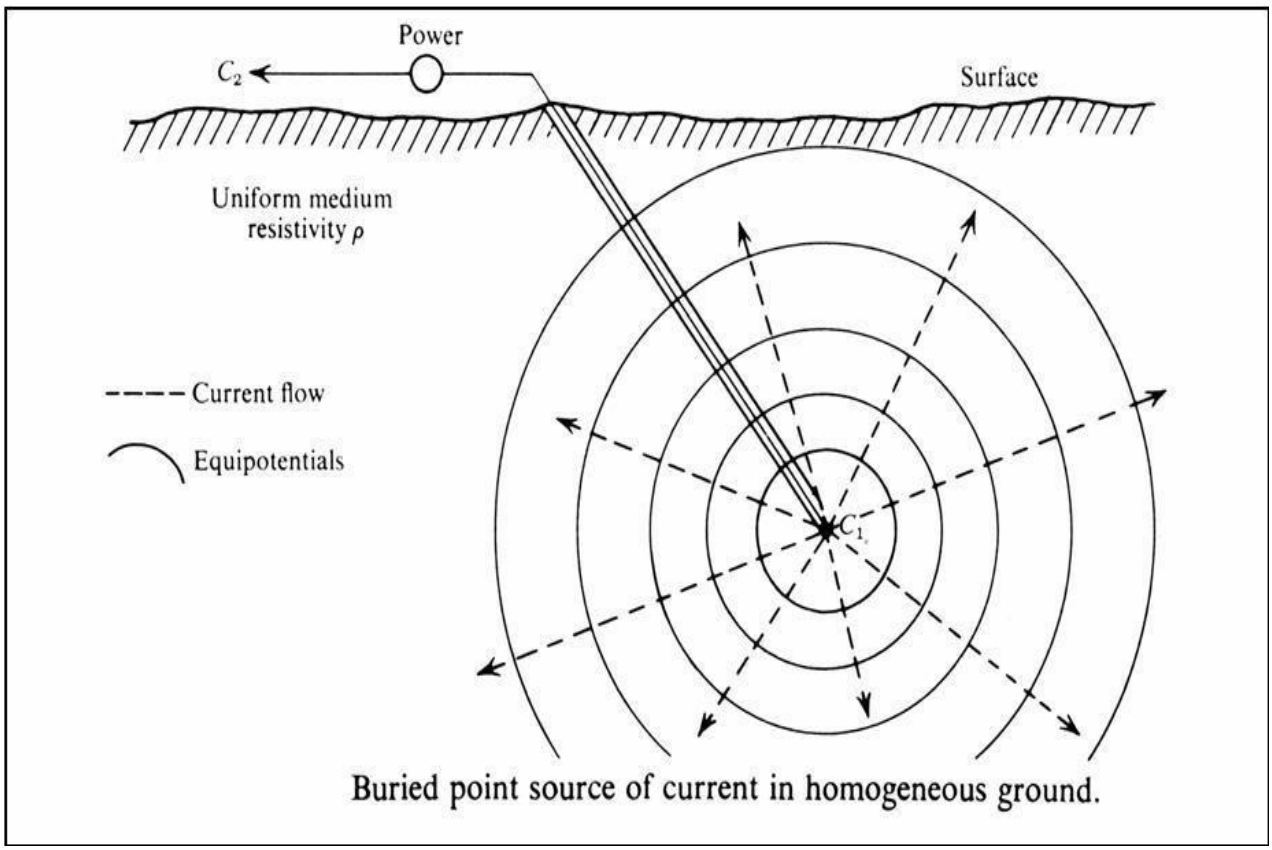

Fig 2.2 Underground current passing into homogenous ground

2.3.3 Electrode configuration

Apparent resistivity values are reliant on the type of electron configuration used as defined by the geometric factor K. There exist three main types of electron configurations which are mostly

named after their inventors which are Frank Wenner and Conrad Schlumberger with also a array of subtypes. The three main types of electron configuration are Wenner array, Schlumberger array and Dipole – Dipole.

Wenner

The array is the most commonly used type (Fig 2.3a) . The subtypes of this array include the standard Wenner, Offset Wenner, Lee- partioningarray and tripotential. In this spread electrode are evenly spaced in a line. From equation (11.0) setting $r_1 = r_{4=a}$ and $r_{2} = r_{3=2a}$ its apparent resistivity

$$\rho_{a=2\pi a\Delta/I} \qquad (2.14)$$

Although the geometry involving this method is modest it has hypothetical shortcomings and is bulky during field work. When undertaking depth investigations its electrodes are spread about a constant centre while *a* the spacing distance is increased. For lateral investigations and mappings, *a* remains the same with all four electrodes moving lengthwise to the line. In mapping apparent resistivity is plotted against the centre of the spread.

Schlumberger

With this array current electrodes are places at a much greater length than potential electrodes (Fig2.3 b).

$r1=(L-x)-l$

$r2=(L+x)+l$

$r_3=(L-x)+l$

and

$r_4=(L+x)-l$

After substituting these values into (equation 11.0) we get

$$\rho_a = \frac{2\pi\Delta V}{I}\left[\left\{\frac{1}{(L-x-l)} - \frac{1}{(L+x)+l}\right\} - \frac{1}{\left\{\frac{1}{(L-x)+l} - \frac{1}{(L+x)-l}\right\}}\right] \quad (2.15)$$

In cases where the distance between the current and potential electrodes is larger than both the two potential electrodes then a first approximation is given

$$\rho_a = \frac{\pi\,(L^2 - X^2)^2}{2l2l(L^2 + X^2)}\left(\frac{\Delta V}{I}\right) \quad (2.16)$$

When dealing with this array it is typically proportioned where x = 0

$$\rho_a \approx \frac{\pi L^2 \Delta V}{2L\ I} \quad (2.17)$$

The substitute symbols for this array is mostly found in works where for example A, B, M, and N are used for the first current electrode second current electrode first potential electrode and second potential electrode respectively. Here L = $\frac{1}{2}$AB and l = $\frac{1}{2}MN$

Dipole – Dipole

In this array potential electrodes thoroughly set apart and distant from the current electrodes which are thoroughly spaced.

$$r_1 = r_4 = 2nl$$
$$r_2 = 2l(n-1)$$
$$r_3 = 2l\,(n+1)$$
$$where\ n > 1$$

By removing the minus,

$$\rho_a = 2\pi\frac{(n-1)n(n+1)l\Delta V}{I} \quad (2.18)$$

This equation is the approximation applied in resistivity surveys. The dipoles may also be positioned broadside, intersected by the traverse line. Here we get

$$r_1 = r_4 = 2\pi l$$

$r_2 = r_3 = 2\{(nl)^2 + l^2)^{1/2} \approx 2nl(1 + 1/2n^2)$ and

$$\rho_a \approx 4\pi n^3 l \Delta V / I \qquad (2.19)$$

Dipole–dipole arrays (Fig 2.3c) have been used extensively by Russian geophysicists since 1950, and especially in Canada, particularly for 'induced polarisation' surveys in mineral exploration, and in the USA in groundwater surveys (Zohdy, 1974)

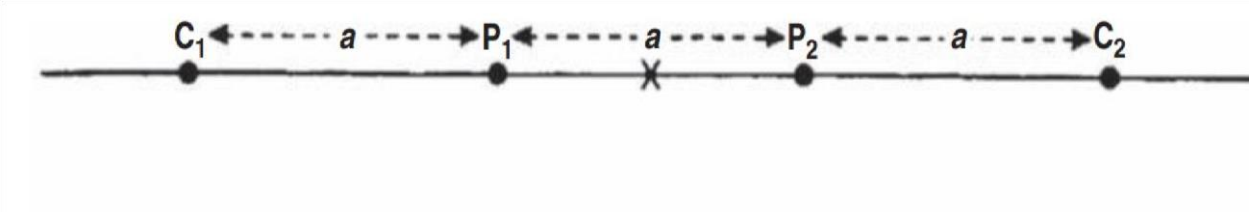

Figure 2.3a Schematic of Wenner array (after Reynolds, 2011)

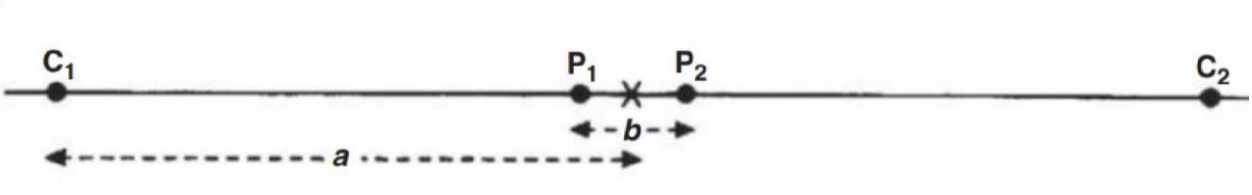

Figure 2.3b Schematic of Schlumberger array (after Reynolds, 2011)

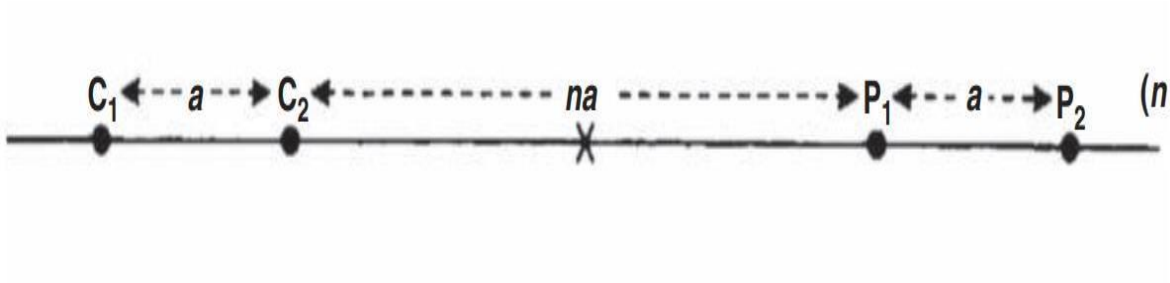

Figure 2.3c Schematic of Dipole-Dipole array (after Reynolds, 2011)

2.3.4 Factors affecting Resistivity of subsurface material

Resistivity is measured in ohm-meter (SI units) with conductivity being its reciprocal. In a case where the conductive material is a cylinder with resistance δR, length δL, and cross-sectional area δA (Fig 2.4a) its resistivity is given as from equation (1.0)

$$\rho = \frac{\delta R \delta A}{\delta L}$$

Resistivity has the most diversity when dealing with geophysical measuring conditions. Minerals like graphite (2.4b) and native minerals are able to conduct electricity with the aid of passing electrons although majority of rock forming minerals are deemed insulators as poor conductors and with electricity being passed via ions present in water. This means that majority of rocks are only able to conduct electricity via electrolytic processes with porosity showing itself to be the most important property when dealing resistivity of rocks with a fair assumption being made that as porosity decreases, resistivity should increase. Because of a variety of rocks available and how similar some may appear to each other it is impossible to identify a rock solemnly on this property (resistivity). An empirical formula provided by Archie demonstrates the relationship between effective porosity, volume and resistivity.

$$\rho = a\Phi^{-m}S^{-n}\rho_w \qquad (2.20)$$

$\boldsymbol{\Phi}$ is the fractional pore volume (porosity), S is the fraction of the pores containing water, ρ_w is the resisitivty of water, $n \approx 2$ with a and m being constants.

Another factor affecting the resistivity of subsurface material is pore connectivity. Subsurface matter that are free of pore spaces indicate high resistivity. Insufficient amount of water will also show high resistive values.

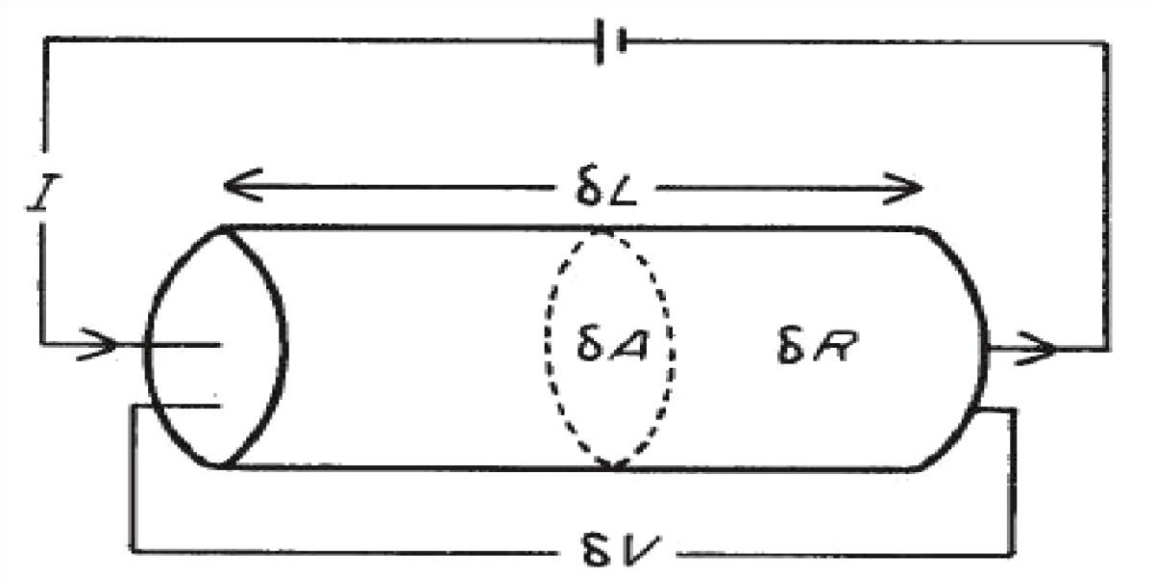

Figure 2.4a parameters used for defining resistivity (From Keary and Brooks 1992)

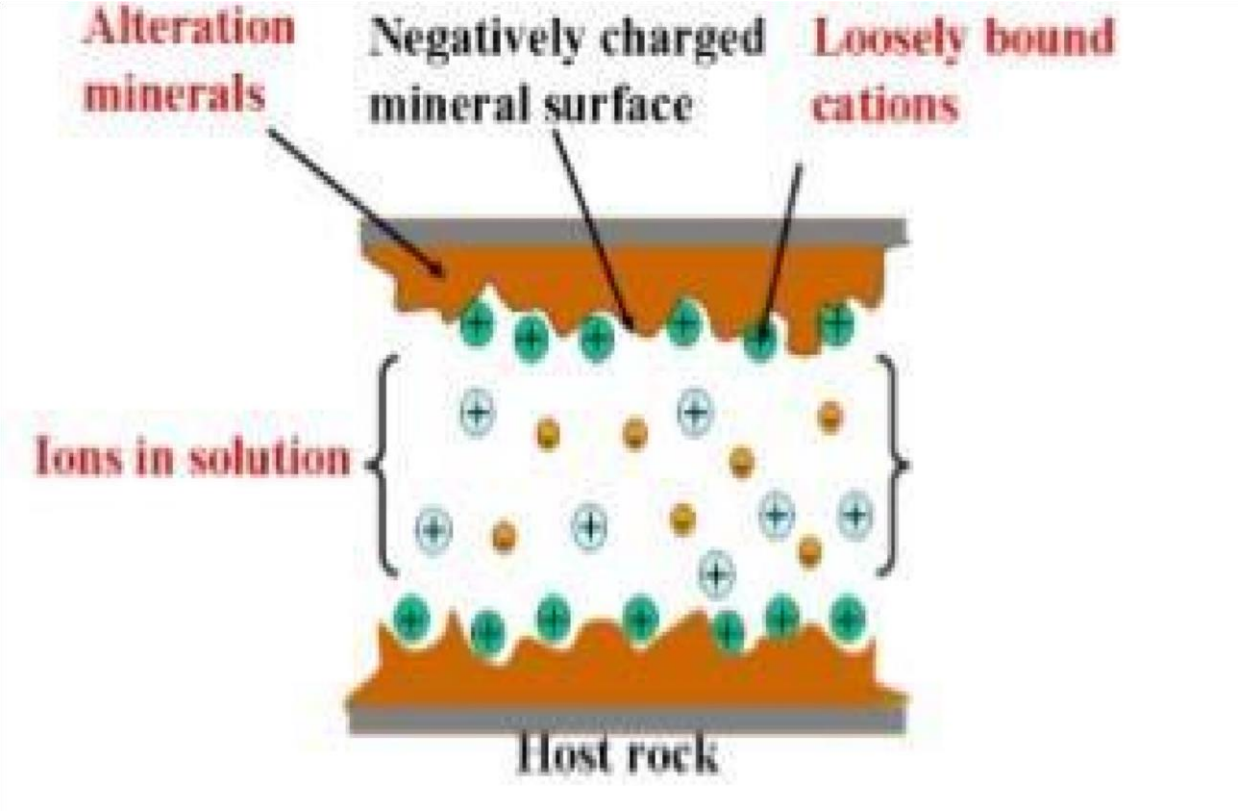

Figure 2.4b Conduction Mechanism (Hersir and Árnason, 2010)
Here is a list of factors affecting resistivity

(i) Geologic Age

(ii) Salinity

(iii) Free ion content of the connate water

(iv) Interconnection of pore spaces (Permeability)

(v) Temperature

(vi) Porosity

(vii) Pressure

(viii) Depth

2.2.5 Limitations of the electrode method

The electrical resistivity method is competent at delineating low layered sequences or vertical discontinuities which contain variations of resistivity values it does suffer from a numerous limitation.

I. Interpretations of resistivity data may be unclear as a result of this geophysical and geological controls are required in order to differentiate between other interpretations

(Kearey *et al,* 2002).

II. Its resolution is limited. Unable to delineate complex structures (Kearey *et al.,* 2002).

III. The grounds topography and the effects of other near surface resistivity variations can cover the effects of deeper variation. (Kearey *et al.,* 2002).

IV. The amount of electrical power generated during the survey has an influence on the probing potential along with the logistics involved in working with very long and heavy cables during surveys (Kearey *et al.,* 2002).

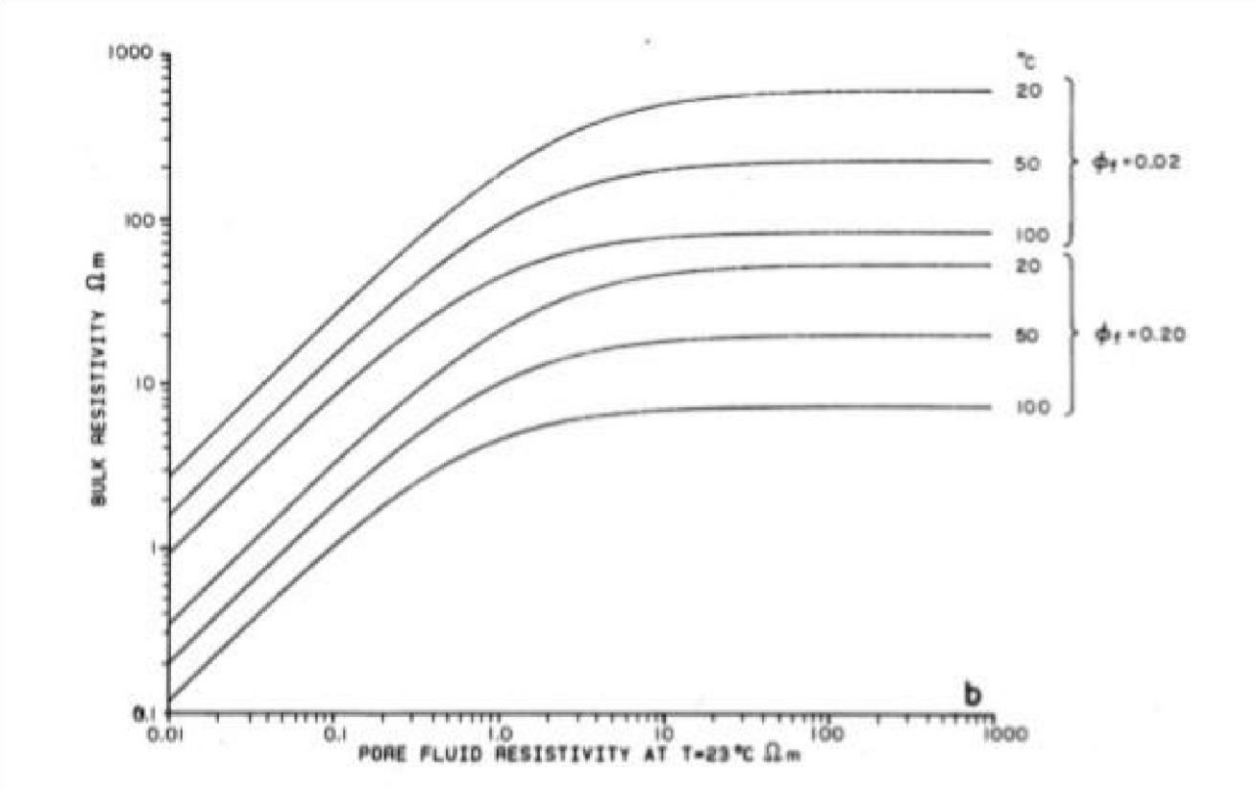

Figure 2.5 shows the relationship between the bulk resistivity and the pore fluid resistivity for different porosities and temperatures for rocks (Flóvenz et al., 1985)

2.4 GROUND PENETRATING RADAR (GPR)

2.4.1 Basic principle of operation

Ground penetrating radar is a geophysical method that attempts to image the subsurface using a high frequency antenna (Brooks et al, 2002). The use of GPR has become favoured most specifically in the engineering sector and archaeology. A GPR system consists of a transmitter

which generates the signal, a receiving antenna and a control desk. The GPR setup spreads the creation of radio waves by the Transmitter antenna Tx. These waves are able to propagate as wide beams. These radio waves travelling at high speeds reach the receiver antenna Rx and return in a matter of few tens to several thousand nanoseconds. The antennas can be used in either monostatic mode or bistatic manner. In the monostatic manner one antenna acts as both the antenna and receiver while in bistatic one antenna is used as transmitter while another will +++++be used as the receiver. The Transmitting antenna Tx is able to bring about radio-waves of a certain frequency as desired by the user estimated at a rate of 50,000 times per second. The receiver is designed to study at a stable rate 32 scans per second which can withstand a duration of a two-way time. This scan usually exhibited on a video screen or graphic recorder. The user will move the antenna across the ground with the receiver antenna displaying the signals as a basis of two-way travel time. The pulse duration of transmitted radio-waves should be short in length in order to produce reflections that be analysed. The major point is that the appearance and feature of the transmitted radio-wave is measurable and noteworthy. If a wave having amplitude is larger than threshold it is displayed as dark on the radar segment. Exhibits can be shown as variable area wiggles or wiggle trace only.

Bright colors indicate strong reflections.

2.4.2 Propagation of radio-waves

The electromagnetic (EM) attributes are connected to their constitution and moisture which are both responsible for the speed of the radio-waves moving through the ground and fading EM

wave. Radio-wave speeds in any channel depending on speed of light in free space (c = 0.3m/ns), its relative dielectric constant (ε_r) and relative magnetic permeability (μ_r = 1 for non-magnetic materials). Favourable outcomes of the technique are dependent on the flexibility of the earth permit the transference of radio waves. Certain materials like saturated clay, water and sea water soak up or throw back to a degree that they appear non-transparent. The difference in dielectric constant linking adjoining layers that make it possible to reflection of incident electromagnetic radiation. The bigger the difference will result in larger amounts of energy reflected. The reflection coefficient (R) which is the portion of energy reflected is a result of the difference in radio-waves velocities and dielectric constants of adjoining mediums. The size of R is ±1 for all instances while portion of energies transferred is identical to 1−R.

Amplitude reflection coefficient is:

$R = \frac{(V_1 - V_2)}{(V_1 + V_2)}$ Where V_1 and V_2 are radio-waves velocities for each layer

$R = \frac{\sqrt{}_2 - \sqrt{}_1}{\sqrt{}_2 + \sqrt{}_1}$ Where ε_1 and ε_2 are corresponding dielectric constants for each layer

2.4.3 Limitations of GPR

Conditional to the effectiveness of GPR are the survey restrictions and the user operating the equipment with the skill and experience of the user being vital. Someone who is not well skilled, knowledgeable and well-practised may make a lot of mistakes while working with the equipment. In scenarios involving opaque framework locations human factors are key in determining a favourable outcome. In scenarios where the data obtained on the site is for later processing this reduces the human factor involvement. After treatment software when used reduces noise in the data which is beneficial because the human factor is removed. Soil type is the largest limitation

when dealing with GPR. Soils like clay which are of a highly conductive nature attenuate radar signals significantly which is a direct correlation with the effective depth of penetration of the EM wave of specific antenna frequencies. Low frequency antenna will provide high potential penetration whilst high frequency antenna will provide will provide lower penetrations. In striking balance lower frequency antennas have to be favoured which will result in the identification of only great targets on the ground. Accurate penetration depths are dependent on circumstances surrounding the location and the earth's conditions which cannot be obtained before starting the study. The type of subsurface material present and surface conditions are also known to distort signal penetration. When the soil contains various articles of dissimilar sizes, dispersing of signals is much evident in these types of scenarios. Water content in the soil also plays a vital role in GPR limitation. Soils that are full of water will likely separate reflections from the GPR details. If the surface constitutes reinforced concrete which has compactly packed bars dispersion of waves will occur, unsteady grounds provide similar results making it increasing difficult to recognize possible targets. This is also applicable to situations of rains when the exterior is filled with water or on the surface coarse gravel is evident (Botteril, 2020).

2.4.4 Advantages of GPR

1) The prime advantage of GPR is due to its various antenna it has the ability to probe and sort out characteristics from a few centimeters to hundreds of meters (Mellet, 1995).

2) The GPR method has the ability to gather huge volumes of data (Hruska et al., 1999)
3) GPR method allows the user to view freshly acquired data on site usually for quality assurance (Mellet, 1995)

4) The capacity of GPR to make use of remote non contacting transducers of radiated energy in contrast to seismic which requires contact with the earth. This is an advantage (Robinson et al, 2013)

CHAPTER THREE

METHODOLOGY

3.1 INTRODUCTION

2D Electrical Resistivity technique and GPR methods were deployed for the subsurface mapping of the two types of contaminants at the two locations. The two contaminants are namely:

i. The first location (MTU female hostel) has a seepage water from soakaway/septic tank ii. The second location is an oil/diesel waste site from a diesel power generating plant close to College of Basic and Applied Sciences

The Electrical method can provide high resistive response or lowly resistive response in the presence of the two types of contaminants investigated in this study. 2D electrical resistivity technique was chosen because it can provide lateral and vertical subsurface electrical resistivity distribution. Likewise, GPR provides vertical and lateral variation in the subsurface and with a very high resolution. GPR is sensitive to variation in subsurface dielectric permittivity and conductivity. Therefore, it is expected that there will be variation in the subsurface properties due to the mentioned contaminants.

3.2 ELECTRICAL RESISTIVITY METHOD

3.2.1 Data Acquisition

The ABEM LS along with 64 steel electrodes and other accessories were used during the 2-D Electrical resistivity data acquisition. The equipment and accessories are listed below:

i. ABEM LS

ii. 64 steel electrodes and clips iii. Four Multicore Cables with 16 current take-out each iv. Hammers

v. Meter Rule vi. GPS vii. 150Ah Deep Cycle Battery

Location 1 (waste water seepage site): Nine (9) traverse lines of 2D ERT were surveyed in total. Four (4) traverse lines with a minimum electrode spacing of 0.5 m each (traverse length of 31.5 m) and Five (5) overlapping traverses were measured with a minimum electrode spacing of 0.2 m (traverse length of 12.6 m). This was done to attain varying resolution and depth of penetration on the observed waste water seepage site. Each of the traverses are 1m apart and Dipole-Dipole array was used because of its lateral resolution and depth of penetration compared to other arrays (Fig 3.1a and 3.2a).

Location 2 (Oil/diesel waste site): An electrode spacing of 0.2 m was used to ensure high subsurface resolution and a traverse length of 6.3 m was achieved. Ten 2D ERT profiles were achieved along seven traverse lines (Fig 3.1b and 3.2b). Lines 3, 4 and 5 had an additional spread of 12.6m measured across it.

Figure 3.1a Set up of ABEM LS during Data acquisition on Location 1

Figure 3.1b Set up of ABEM LS during Data acquisition on Location 2

3.2.3 Data Processing

The data was downloaded in .dat format which was uploaded into the AGI Earthimager software for processing and 2D inversion. The smooth model technique was selected for the inversion and about three iterations were carried out. The field data and the calculated model pseudosections are then iterated to generate a 2D inverted resistivity section (Fig 3.3). The 2D inverted resistivity section is in a colour coded format of which the horizontal scale is the lateral distance, the vertical scale is the investigated depth while the colour scale bar are the resistivity values allotted to each of the colours in the 2D inverted section.

3.3 GROUND PENETRATING RADAR

3.3.1 Data Acquisition

Mala Pro Explorer Ground Penetrating Radar was deployed for the GPR measurements. The equipment and accessories are listed below:

i. MALA Ground Explorer with Monitor control unit ii.
Shielded Antennas (160 and 450 MHz) with DGPS and Battery iii.
Rough terrain cart

160 MHz and 450 MHz antennas were used during the data acquisition of this method to attain good resolution and depth of penetration as conductive layer will negatively impact the depth of penetration in GPR methods. The antennas were placed in the rough terrain cart which was pushed gently along the traverse and data were obtained in the process. This is done repeatedly until all traverses were surveyed.

Location 1 (waste water seepage site): At the location 1, the (4) lines that were covered during the 2D Electrical Resistivity were occupied by the GPR method with both 160 MHz and 450 MHz antennas. Each of these lines are 1m apart and about 33m long. This was done for proper correlation and integration of both methods (Fig 3.2a).

Location 2 (Oil/diesel waste site at the diesel generating plant): At this location, eight (8) lines were worked on with antennas 160 MHz and 450 MHz the final line on this location was a middle line running from N-S at frequency 450 MHz (Fig 3.2b).


3°23′31.67″E
3°24′35.40″E
6°43′48.18″N
6°43′48.05″N
DATA ACQUISITION MAP
2D ERT AND GPR LINES
Legend
2D ERT LINES
SP
Female hostel
Google Earth
20 m
N
6°43′45.64″N
6°43′45.63″N
3°24′35.37″E

Figure 3.2a Map showing survey layout of the 2D resistivity and GPR traverses at Location 1

Figure 3.2b Map showing survey layout of the 2D resistivity and GPR traverses at Location 2

Figure 3.3 Set up of the MALA Ground Explorer GPR with the 160 MHz prior to data acquisition

3.3.4 Data processing

The raw field data were processed using ReflexW and GPR viewer. Gain control, time zero adjustment, background removal, and topographic corrections were also applied. The crucial focus when processing raw GPR data is signal resolution improvement which could help during interpretation. The main aim of using gain control during processing method is to increase all amplitudes that were observed to be low. Background removal removes the background noise or DC effect thereby improving the resolution of the image and produces better insight into the subsurface. Time zero adjustments make it possible to determine the depth of the contamination by modifying time traces to a mutual point.

CHAPTER FOUR

RESULT AND DISCUSSION

4.1 RESULTS

The result of the electrical resistivity method has been presented as interpreted 2D inverted resistivity sections in Figs 4.1 to 4.4 in location 1 and Figs 4.13 to 4.18 in location 2. Similarly, the result of the processed GPR sections in location 1 has been presented as interpreted radargram sections in Figs 4.8 to 4.12 while that of location 2 are presented in Figures 4.19 to 4.26. The result of the 3D inverted resistivity of the parallel 2D ERT lines in location 1 has been presented as an interpreted 3D resistivity cubes in Figures 4.5 to 4.7.

4.2 DISCUSSION OF RESULTS

4.2.1 DISCUSSION OF 2D ERT RESULTS IN LOCATION 1

4.2.1.1 Traverse 1

Fig 4.1a is the interpreted 2D inverted resistivity section on Traverse 1 with minimum electrode spacing of 0.5m while Fig 4.1b is the interpreted 2D ERT with 0.2m minimum electrode spacing.

In Fig 4.1a, the subsurface resistivity ranges from about 11 to 130 Ωm and an average depth of about 6.9m was investigated over a lateral distance of about 33.3m. The subsurface can be divided into two major layers based on vertical and lateral variation in subsurface resistivity distribution.

The first region is with varying resistivity range of 11 to 130 Ωm and delineated to a depth range of 2.55 to 3.4m. Regions with low resistivity range of 11 to 21 Ωm are descriptive of waste water polluted regions and is prominent within the lateral distance of about 0 to 17m after which relatively high electrical resistivity range of 38 to 130 Ωm is observed which is expressive of

unpolluted topsoil/lateritic soil at the time of investigation. The second geoelectric layer is with resistivity range of 21 to 38 Ωm which is suggestive of lateritic soil/ clayey sand and delineated to an average depth of about 6.9m.

Line 1b (Fig 4.1b) has provided a higher-resolution image of the subsurface electrical resistivity distribution along Line 1 within a lateral distance of 12.6m and an average depth of about 2.76m.

Similarly, regions with low resistivity range of 10 to 20 Ωm are indicative of waste water polluted regions while regions with relatively high electrical resistivity range of 28 to 82 Ωm are expressive of unpolluted Topsoil/Lateritic Soil at the time of investigation. The low resistivity anomaly structure observed at a lateral distance of about 6m and depth of about 0.69m can be associated to the buried pipe containing the waste water.

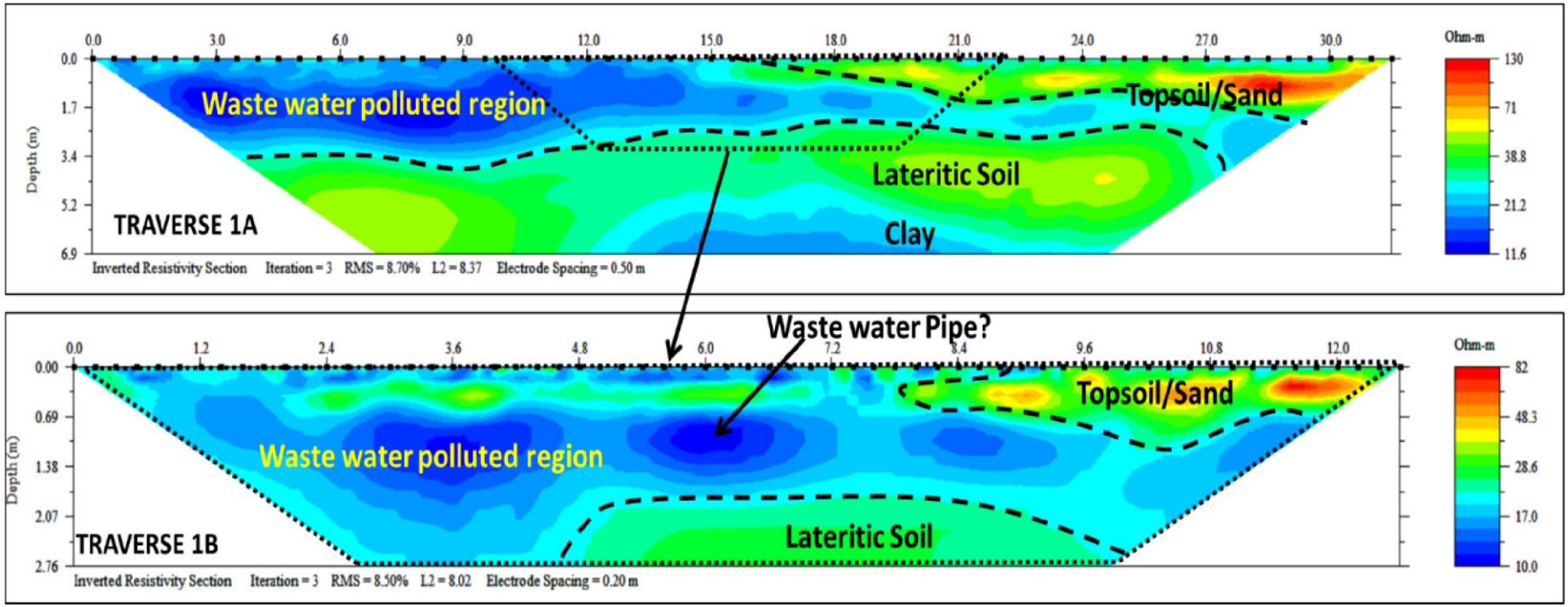

Figs 4.1: Interpreted 2D inverted Electrical Resistivity along Traverse 1 with (a) 0.5m minimum spacing (b) 0.2 m minimum electrode spacing showing identified features around the waste water seepage site

4.2.1.2 Traverse 2

Fig 4.2a is the interpreted 2D inverted resistivity section on Traverse 2 with minimum electrode spacing of 0.5m while Fig 4.2b is the interpreted 2D ERT with 0.2m minimum electrode spacing.

In Fig 4.2a, the subsurface resistivity ranges from about 6.4 to 102 Ωm and an average depth of about 6.9m was investigated over a lateral distance of about 33.3m. The subsurface can be divided into two major geoelectric layers based on vertical and lateral variation in subsurface resistivity distribution. The first region is with varying resistivity range of 6.4 to 102 Ωm and delineated to a depth range of 1.69 to 3.4m. Regions with low resistivity range of 6.4 to 19 Ωm are descriptive of waste water polluted regions and is prominent within the lateral distance of about 0 to 16.5 m after which relatively high electrical resistivity range of 25 to 102 Ωm is observed which is expressive of unpolluted topsoil/lateritic soil at the time of investigation. The second geoelectric layer is with electrical resistivity range of 25.4 to 102 Ωm which is suggestive of lateritic soil and delineated to an average depth of about 6.9m.

Line 2b (Fig 4.2b) has provided a higher-resolution image of the subsurface electrical resistivity distribution along Line 2 within a lateral distance of 12.6m and an average depth of about 2.76m.

Similarly, regions with low resistivity range of 10.8 to 18 Ωm are indicative of waste water polluted regions while regions with relatively high electrical resistivity range of 25.4 to 96 Ωm are expressive of unpolluted Topsoil/Lateritic Soil at the time of investigation. The low resistivity anomaly structure observed at a lateral distance of about 5.2m and depth of about 1.1m can be associated to the buried pipe containing the waste water.

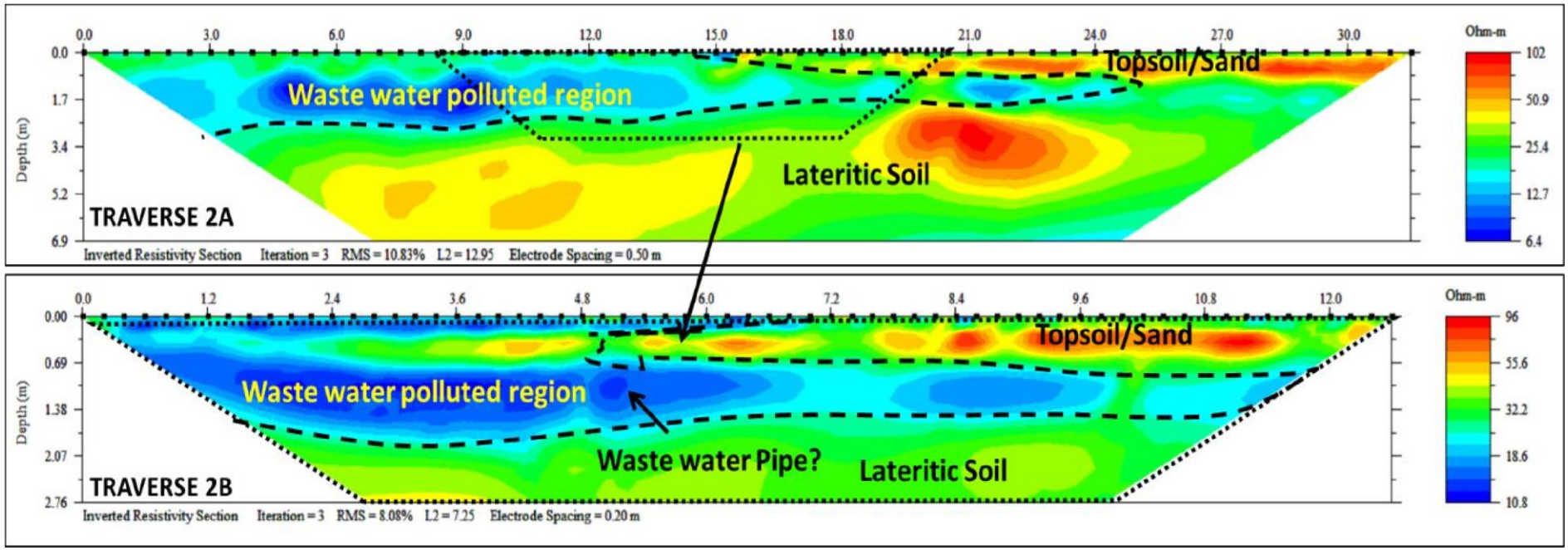

Figs 4.2: Interpreted 2D inverted Electrical Resistivity along Traverse 2 with (a) 0.5m minimum spacing (b) 0.2 m minimum electrode spacing showing identified features around the waste water seepage site

4.2.1.3 Traverse 3

Fig 4.3a is the interpreted 2D inverted resistivity section on Traverse 3 with minimum electrode spacing of 0.5m while Fig 4.3b is the interpreted 2D ERT with 0.2m minimum electrode spacing.

In Fig 4.3a, the subsurface resistivity ranges from about 8 to 138 Ωm and an average depth of about 6.9m was investigated over a lateral distance of about 33.3m. The subsurface can be divided into two major layers based on vertical and lateral variation in subsurface resistivity distribution.

The first region is with varying resistivity range of 8 to 68 Ωm and delineated to a depth range of 0.85 to 3.6m. Regions with low resistivity range of 8 to 25 Ωm are descriptive of waste water polluted regions and is prominent within the lateral distance of about 0 to 30.5 m. Meanwhile, observed relatively high electrical resistivity range of 33 to 138 Ωm is expressive of unpolluted topsoil/lateritic soil at the time of investigation. The second geoelectric layer is with resistivity range of 25 to 103 Ωm which is suggestive of lateritic soil/ clayey sand and delineated to an average depth of about 6.9m.

Line 3b (Fig 4.3b) has provided a higher-resolution image of the subsurface electrical resistivity distribution along Line 3 within a lateral distance of 12.6m and an average depth of about 2.76m.

Regions with low resistivity range of 8 to 21 Ωm are indicative of waste water polluted regions while regions with relatively high electrical resistivity range of 54 to 248 Ωm are expressive of unpolluted Topsoil/Lateritic Soil at the time of investigation. The subtle low resistivity anomaly structure observed at a lateral distance of about 4.8m and depth of about 1.4 m can be associated to the buried pipe containing the waste water.

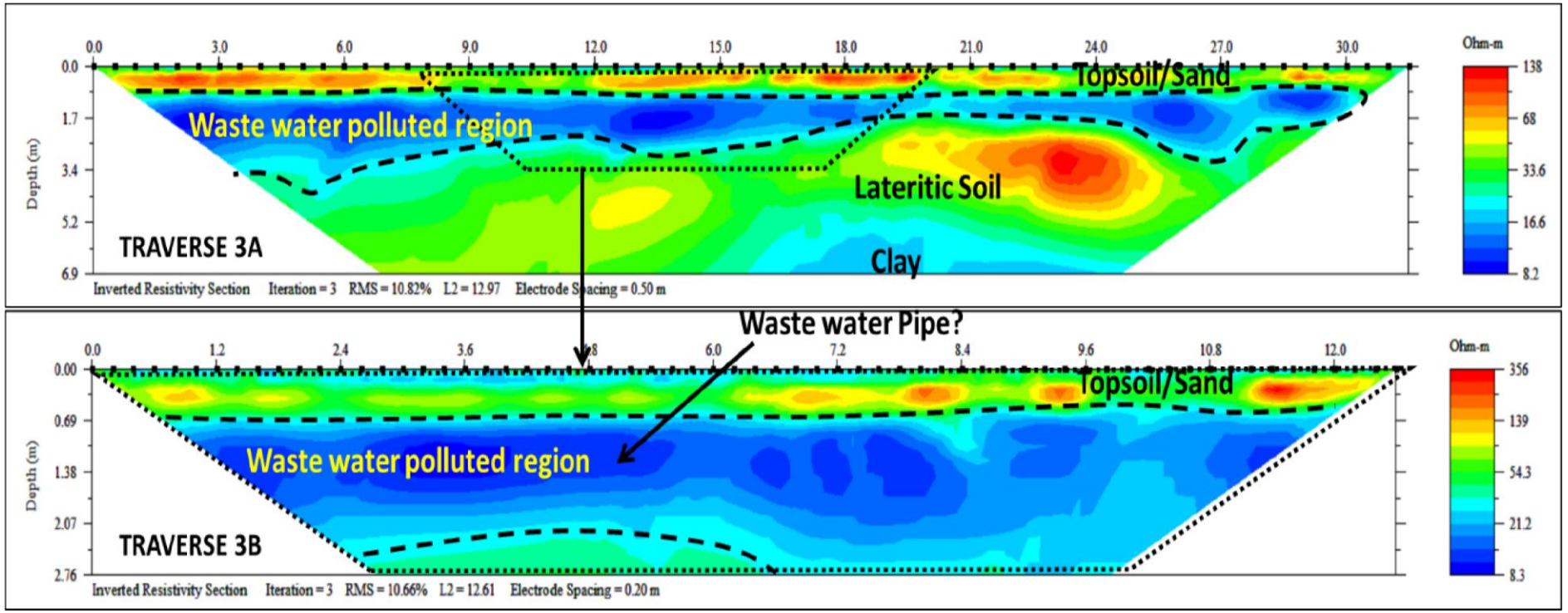

Figure 4.3: Interpreted 2D inverted Electrical Resistivity along Traverse 3 with (a) 0.5m minimum spacing (b) 0.2 m minimum electrode spacing showing identified features around the waste water seepage site

4.2.1.4 Traverse 4

Fig 4.4a is the interpreted 2D inverted resistivity section on Traverse 4 with minimum electrode spacing of 0.5m while Fig 4.4b is the interpreted 2D ERT with 0.2m minimum electrode spacing.

In Fig 4.4a, the subsurface resistivity ranges from about 4 to 187 Ωm and an average depth of about 6.9m was investigated over a lateral distance of about 33.3m. The subsurface can be divided into two major layers based on vertical and lateral variation in subsurface resistivity distribution.

The first region is with varying resistivity range of 4 to 130 Ωm and delineated to a depth range of 0.3 to 3.4m. Regions with low resistivity range of 4 to 19 Ωm are descriptive of waste water polluted regions while regions with relatively high electrical resistivity range of 28 to 187 Ωm is expressive of unpolluted topsoil/lateritic soil at the time of investigation. The second geoelectric layer is with resistivity range of 28 to 120 Ωm which is suggestive of lateritic soil/ clayey sand and delineated to an average depth of about 6.9m.

Line 4b (Fig 4.4b) has provided a higher-resolution image of the subsurface electrical resistivity distribution along Line 4 within a lateral distance of 12.6m and an average depth of about 2.76m.

Low resistivity regions (1 to 29 Ωm) are indicative of waste water polluted regions while regions with relatively high electrical resistivity range of 90 to 866 Ωm are expressive of unpolluted topsoil/Lateritic Soil at the time of investigation. The low resistivity anomaly structure observed at a lateral distance of about 5.8m and depth of about 1.4 m can be descriptive of the buried pipe containing the waste water.

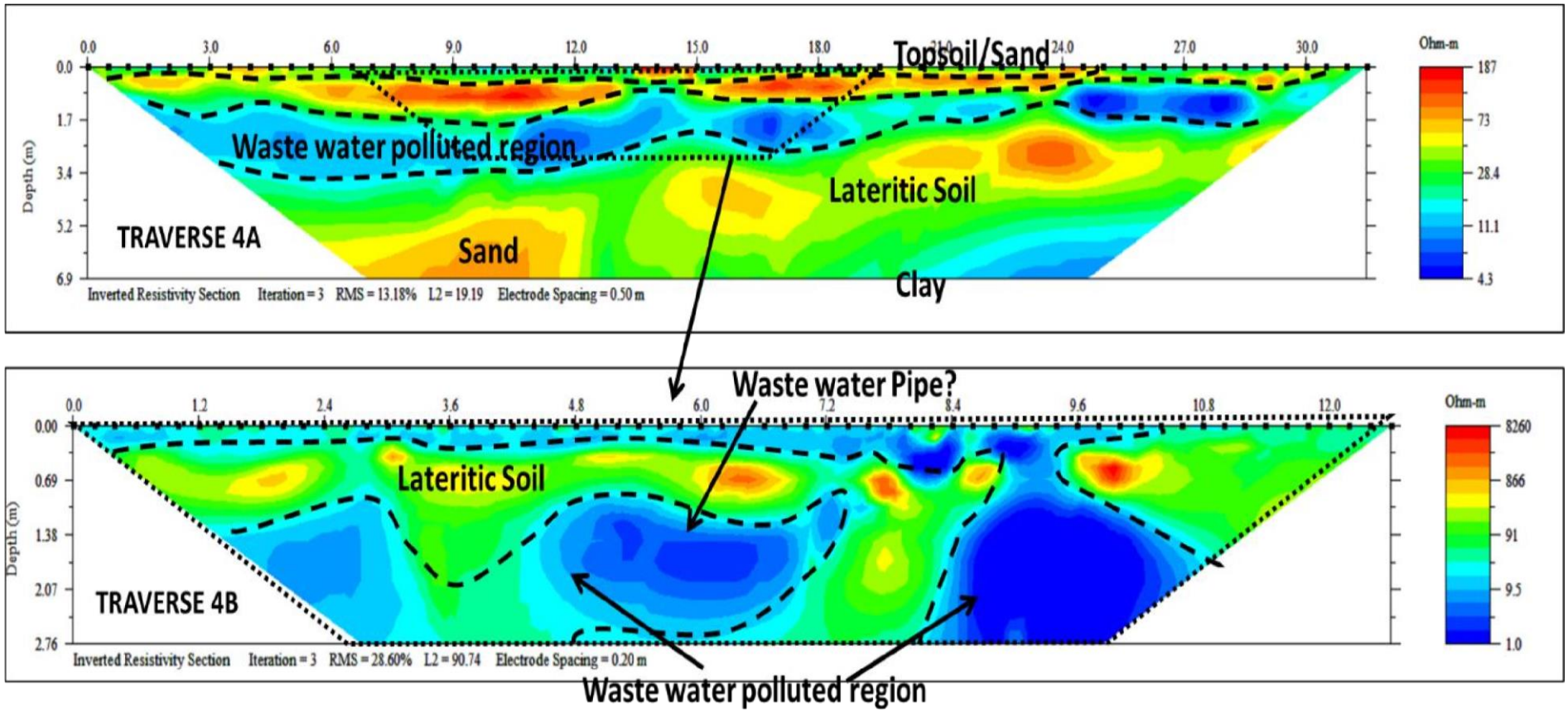

Figure 4.4: Interpreted 2D inverted Electrical Resistivity along Traverse 4 with (a) 0.5m minimum spacing (b) 0.2 m minimum electrode spacing showing identified features around the waste water seepage site

4.2.2 DISCUSSION OF 3D ERT RESULTS IN LOCATION 1

The result of the 3D inverted resistivity cube obtained from the parallel 2D ERT lines have shown the variation in electrical resistivity distribution in 3D view (Figs 4.5 a and b). The observed low resistivity distribution on the surface is consistent with the area covered by the waste-water on the investigated site. In Fig 4.5b, the subsurface region saturated by the waste water seepage can be characterised from its relatively low electrical resistivity distribution of about 13 to 25 Ωm and to a delineated depth of about 2.64 m.

Dynamic slices taken at depth of about 0.1m (Fig 4.6a) and depth of about 1 m (Fig 4.6b) has shown a wider spread of the waste water in the deeper subsurface (Fig 4.6b) compared to surface observations (Fig 4.6a).

The 3D resistivity contour plot has been used to isolate specific subsurface resistivity signatures (Fig 4.7a). This has shown the 3D surfaces of the low resistivity anomalies associated to the waste water seepage (Fig 4.7b).

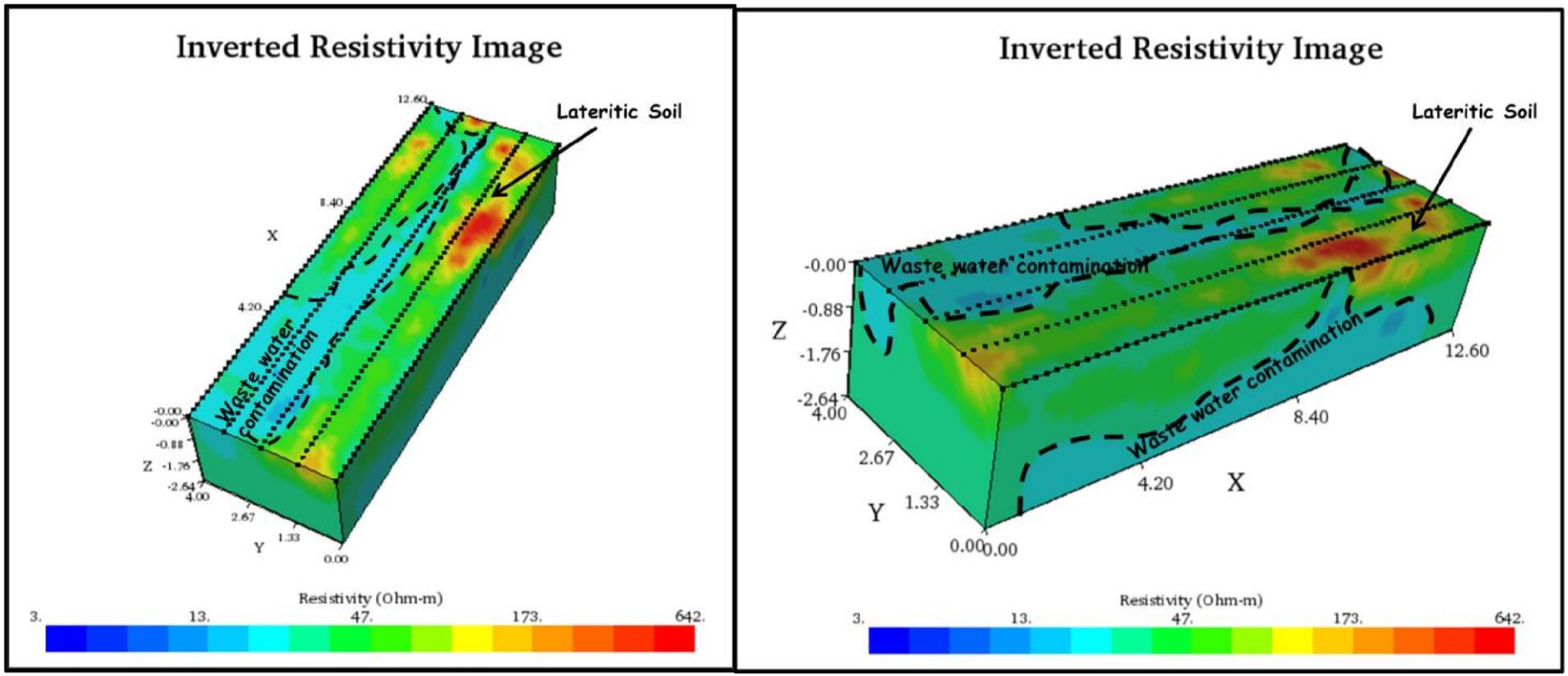

Fig 4.5a and b. Interpreted 3D resistivity cube (from the 2D ERT) lines showing the possible extent of the waste water contamination

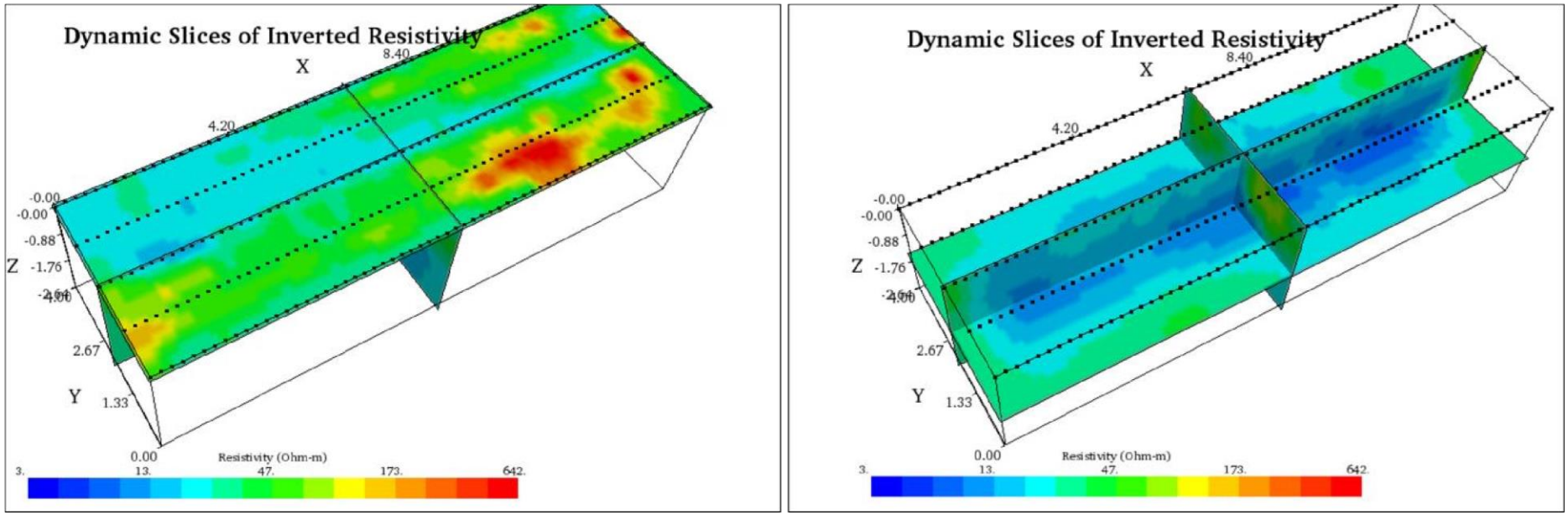

Fig 4.6. Interpreted Dynamic slices of 3D Electrical Resistivity (from the 2D ERT) showing resistivity variations showing the possible extent of the waste water contamination (a) at 0.1m depth (b) at 1m depth

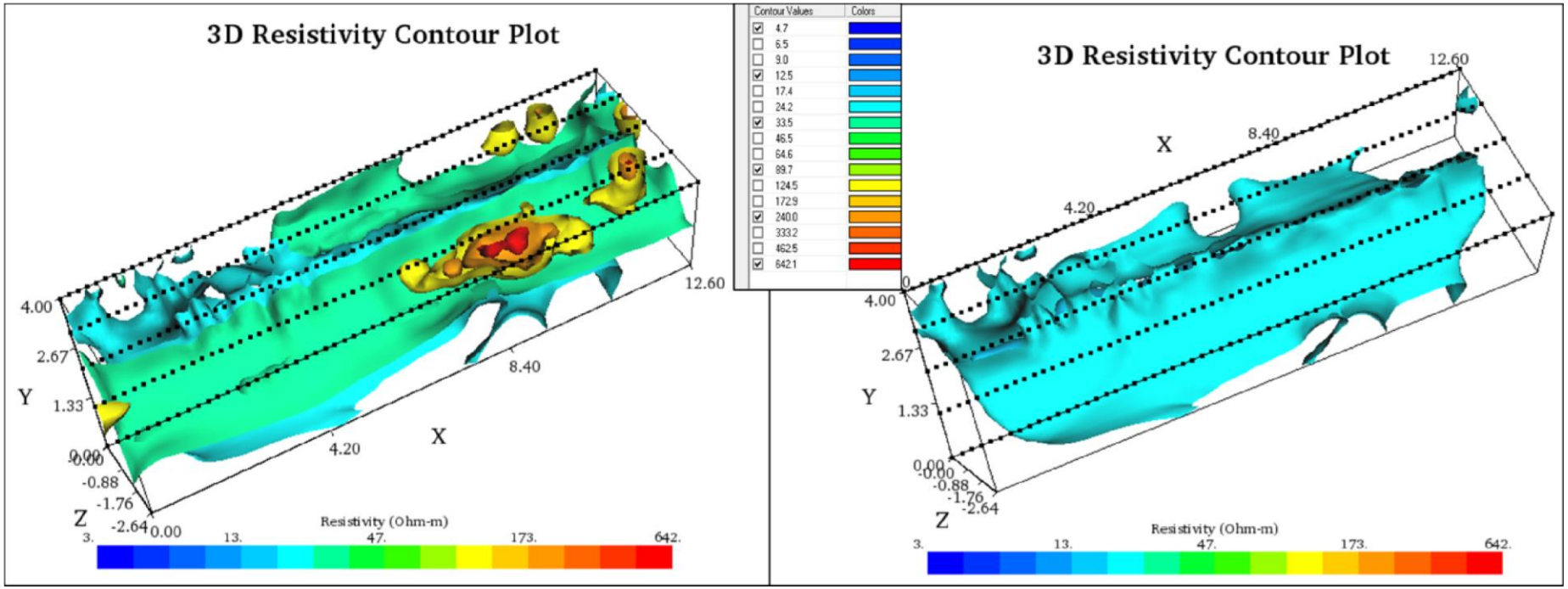

Fig 4.7 Interpreted 3D Iso-Resistivity surfaces of some selected resistivity signatures (a) selected high and low resistivity signatures (b) low resistivity surfaces indicative of waste water polluted regions

4.2.3 DISCUSSION OF GPR RESULTS IN LOCATION 1

4.2.3.1 Traverse 1

The interpreted 2D radargram along traverse 1 is presented in Fig 4.8. Relatively high amplitude anomaly can be observed at a depth range of 1.2 to 2.1 m. The relatively high amplitude can be associated to higher water saturation (increased reflection or re-echoed energy) due to the seepage of the waste water. At lateral distance of about 2m and depth of about 0.3m, hyperbolic signatures can be observed which is indicative of buried cable or reflection from overhead metallic solar electric pole on the site. Similarly, hyperbolic signature expressive of possible plastic pipe can be observed at a lateral distance of about 12.8m and depth of about 0.3m. This pipe has not been exposed and can be one of the pipes that is leaking the waste water. At lateral distance of about 24m multiple hyperbolas can be observed which is expressive of both concrete and pipe. This pipe can be observed around a manhole around this area and can be one of the waste-water pipes that are leaking waste water in the investigated area. Meanwhile, other possibilities such as damaged underground concrete septic tank can add up to the observed widespread of waste water saturation along the traverses.

4.2.3.2 Traverse 2

The interpreted 2D radargram along traverse 2 is presented in Fig 4.9. Relatively high amplitude anomaly can be observed at a depth range of 1.2 to 2.0 m which can be associated to higher water saturation (results in increased reflection or re-echoed energy) due to the seepage of the waste water. At lateral distance of about 15m, hyperbolic signature expressive of possible plastic pipe can be observed at a depth of about 0.3m. High reflection anomalies are observed around

the pipe indicative of leaking the waste water. At lateral distance of about 22 m hyperbolas can be observed which is expressive of pipe.

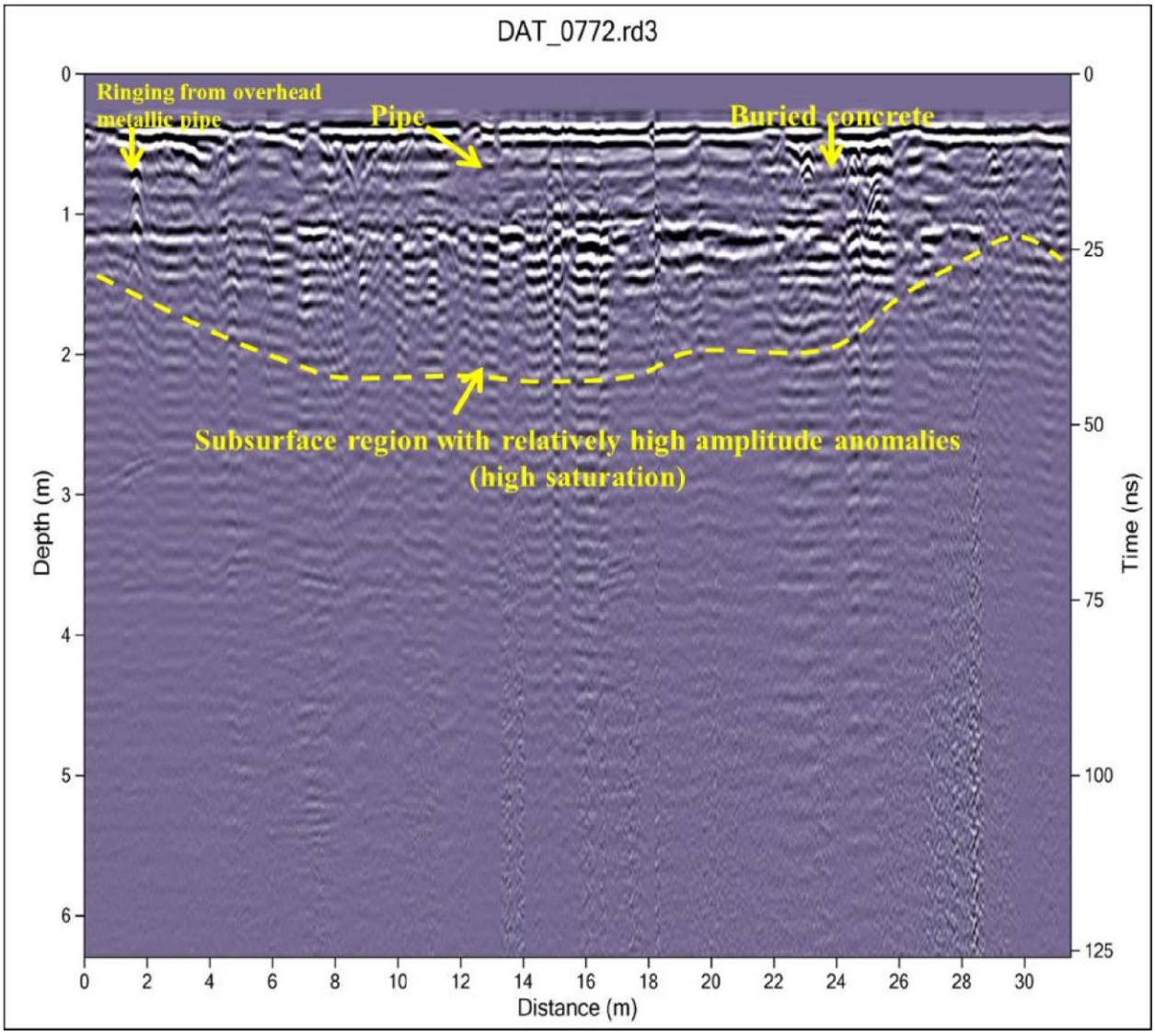

Figure 4.8 Interpreted GPR radargram using the 450 MHz antenna along traverse 1 at Location 1.

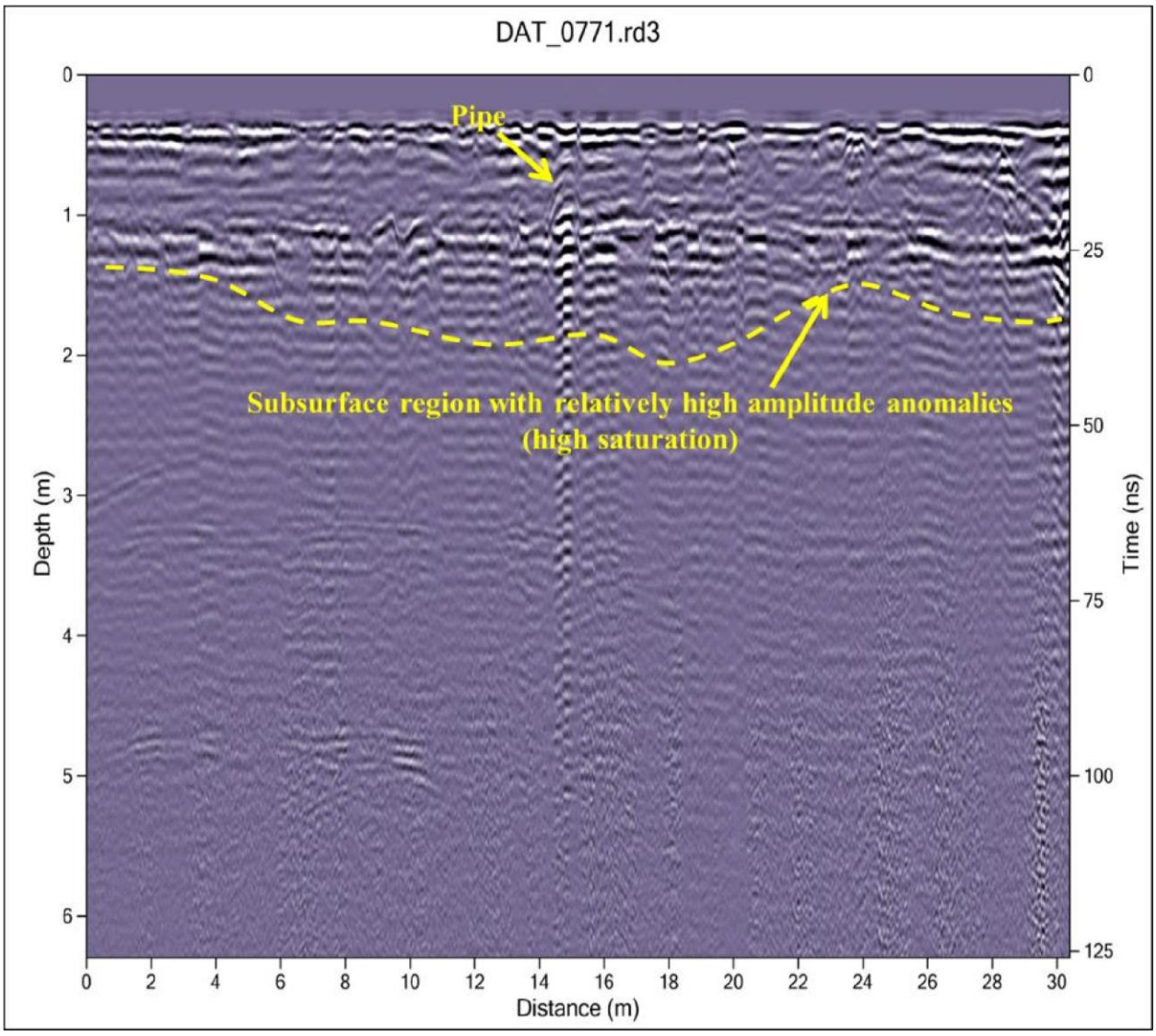

Figure 4.9 Interpreted GPR radargram using the 450 MHz antenna along Traverse 2 at Location 1.

4.2.3.3 Traverse 3

The interpreted 2D radargram along traverse 3 is presented in Fig 4.10. Relatively high amplitude anomaly can be observed at a depth range of 1.5 to 2 m which can be expressive of higher water saturation (increased reflection or re-echoed energy) due to the seepage of the waste water. Hyperbolic signatures expressive of possible plastic pipe can be observed at a lateral distance of about 17m and depth of about 0.4 m. This pipe can be one of the pipes leaking the waste water.

4.2.3.4 Traverse 4

The interpreted 2D radargram along traverse 4 is presented in Fig 4.11. Relatively high amplitude anomaly can be observed at a depth range of 1.2 to 1.9 m which is indicative of higher water saturation (results in increased reflection or re-echoed energy) as a result of the seepage of the waste water. At lateral distance of about 18 m, hyperbolic signatures suggestive of possible plastic pipe can be observed at a depth of about 0.5 m. The relatively higher reflection anomalies observed around this pipe is suggestive of one of the possible sources of the leaking waste water.

4.2.3.5 Correlation of GPR traverses

The correlated GPR traverses in Location 1 is presented in Figure 4.12. Higher amplitude anomalies can be observed on the Lines as one traverses away from the source or exit of the pipe (east to west). This can be associated to increased saturation of the waste water on the lines

closer to the exit or buried concrete storage for waste water. Therefore, beyond damaged pipe, the buried concrete waste water reservoir might have been compromised and could be one of the possible sources of the waste water.

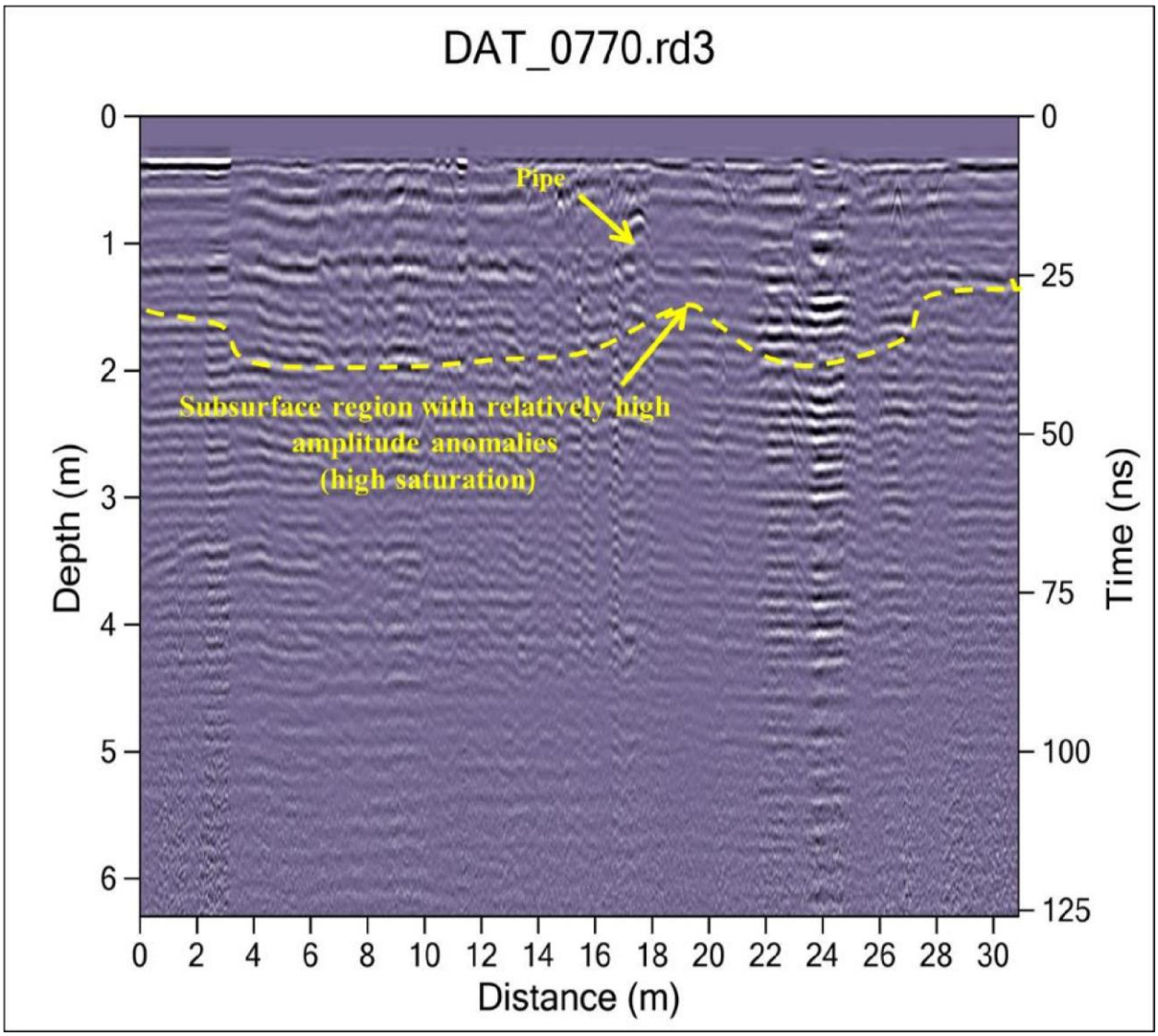

Figure 4.10 Interpreted GPR radargram using the 450 MHz antenna along Traverse 3 at Location

1.

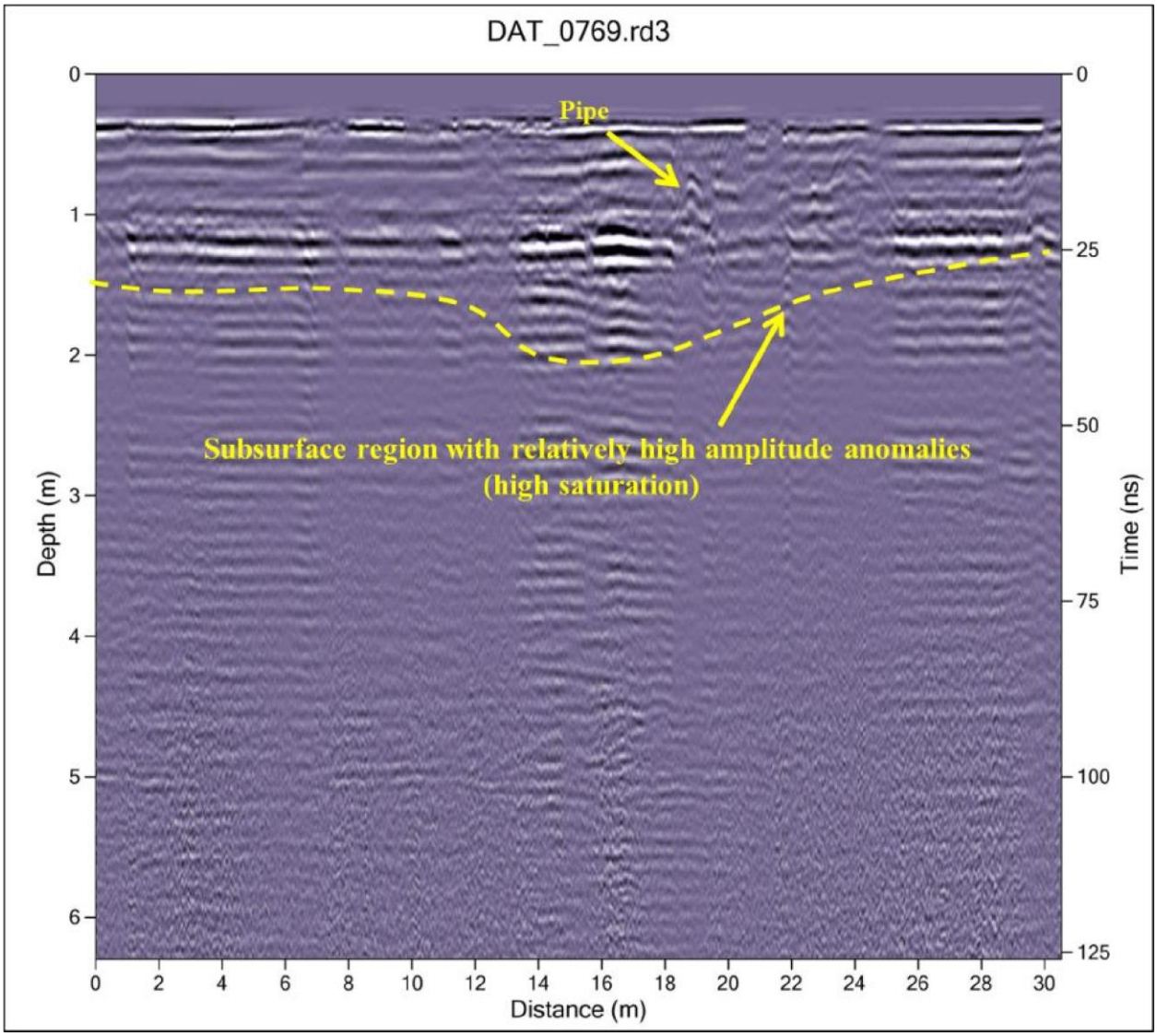

Figure 4.11 Interpreted GPR radargram using the 450 MHz antenna along Traverse 4 at Location 1

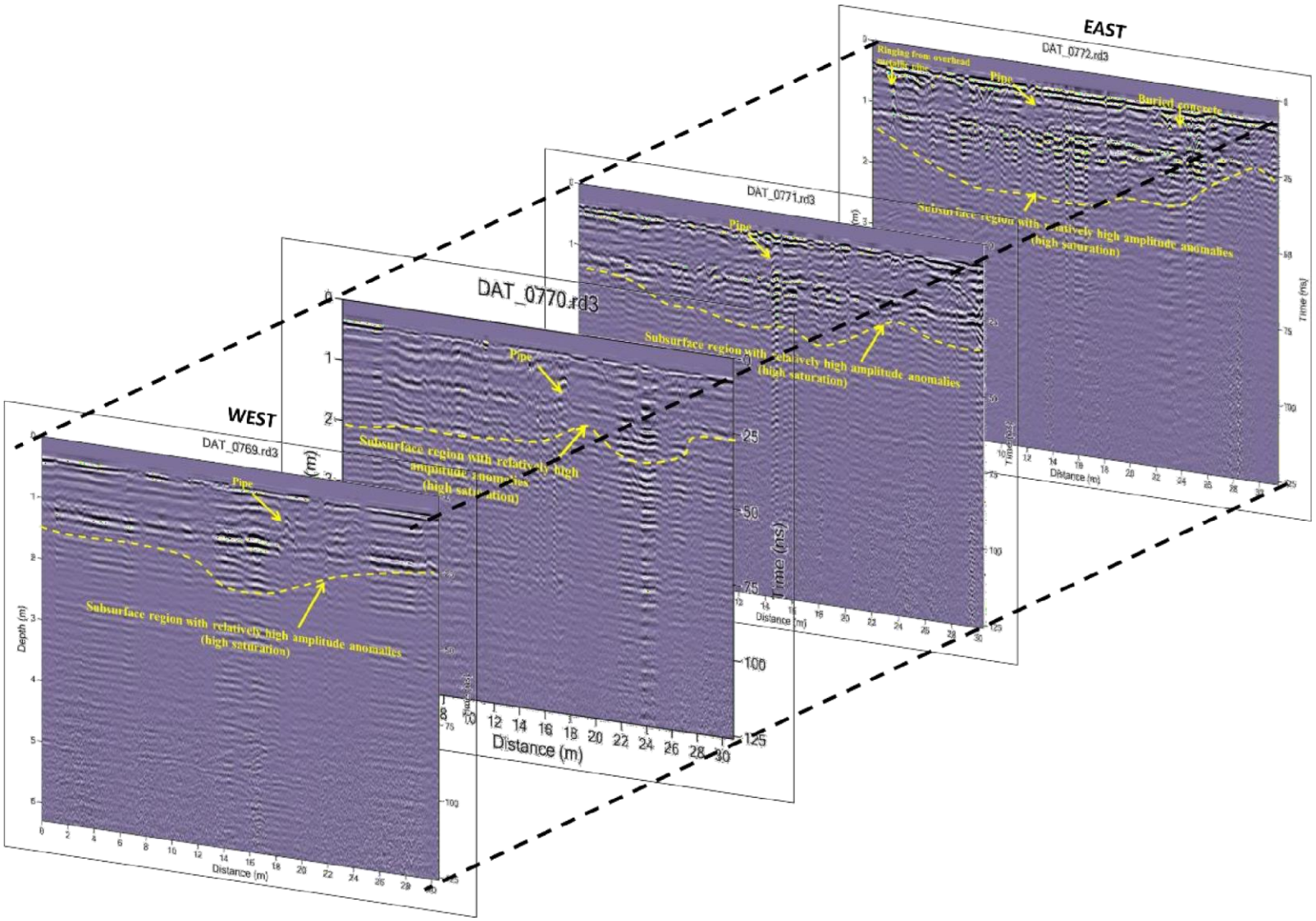

Figure 4.12 3D augmented view and correlation of interpreted parallel GPR Lines in Location 1

4.2.4 DISCUSSION OF 2D ERT RESULTS IN LOCATION 2

4.2.4.1 Traverse 1

Figure 4.13a represents the interpreted inverted 2D electrical resistivity section along Traverse 1 in location 2. The subsurface resistivity along this section ranges from about 7 to 572 Ωm and a depth of about 1.38 m was investigated. The 2D electrical resistivity section can be characterized into three main geoelectric layers based on its vertical and lateral variation in electrical resistivity values.

The first region is with resistivity range of 7 to 67Ωm and delineated to a depth range of 0.1 to 0.15m. The region comprises of the topsoil, the visibly oil/diesel contaminated region and humus/water wet surface region. The relatively low resistivity signatures within this region can be partly due to water-wet surfaces after precipitation or biogenically degraded surficial oil/diesel waste. The second geoelectric layer is with relatively high electrical resistivity range of 114 to 572 Ωm which is expressive of oil/diesel waste and delineated to a depth range of 0.45 m to 0.55 m at the time of investigation. This region constitutes the suspected subsoil region that has been contaminated by the oil/diesel waste and may therefore require mitigation measures to avoid further percolation of oil/diesel waste. The third geoelectric layer is with electrical resistivity range of 39 to 114 Ωm which can be associated to the lateritic soil and delineated to an average depth of about 1.38m.

4.2.4.2 Traverse 2

Figure 4.13b represents the interpreted inverted 2D electrical resistivity section along Traverse 2 in location 2. The subsurface resistivity along this section ranges from about 6 to 1020 Ωm and a depth of about 1.38 m was investigated. The 2D electrical resistivity section can be characterized

into three main geoelectric layers based on its vertical and lateral variation in electrical resistivity values.

The first region is with resistivity range of 6 to 50 Ωm and delineated to a depth range of 0.1 to 0.14 m. This region comprises of the topsoil, the visibly oil/diesel contaminated region and humus/water wet surface region. The relatively low resistivity signatures within this region can be partly due to water-wet surfaces after precipitation or biogenically degraded surficial oil/diesel waste. At a lateral distance of about 0 to 4m, the second geoelectric layer is characterised by relatively high electrical resistivity range of 181 to 1020 Ωm which is expressive of oil/diesel waste and delineated to a depth range of 0.3 m to 0.7 m at the time of investigation. This region constitutes the suspected subsoil region that has been contaminated by the oil/diesel waste. The high resistivity (284 to 1020 Ωm) anomalies observed at lateral distance of about 5.8 to 6.3m can be due to buried concrete or gravels observed on the field during data

acquisition. The third geoelectric layer is with electrical resistivity range of 50 to 181 Ωm which can be associated to the lateritic soil and delineated to an average depth of about 1.38m.

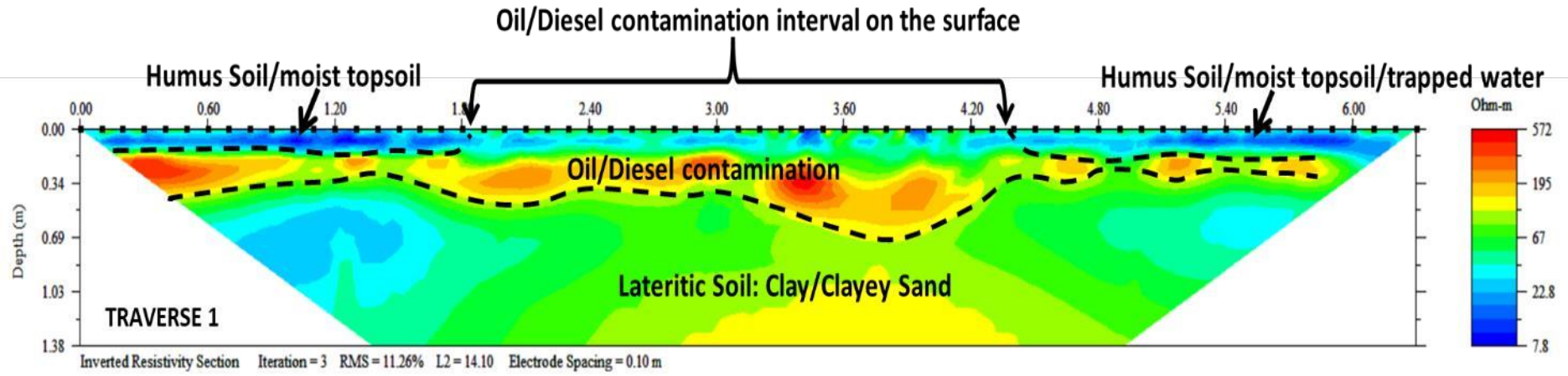

Figure 4.13a. Interpreted 2D inverted resistivity section on Traverse1

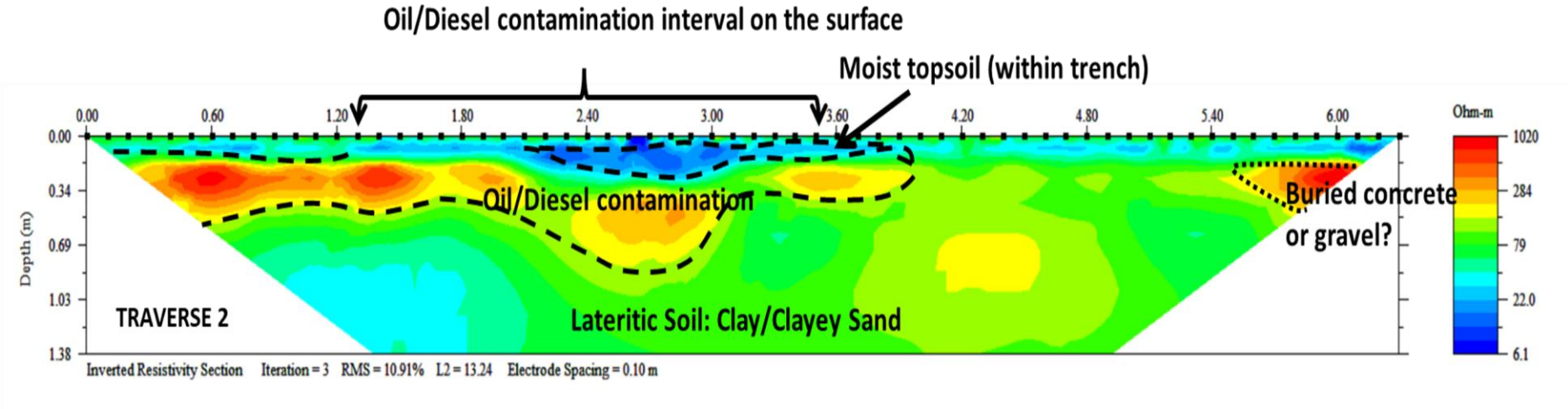

Figure 4.13b. Interpreted 2D inverted resistivity section on Traverse2

4.2.4.3 Traverse 3

Figure 4.14a represents the interpreted inverted 2D electrical resistivity section along Traverse 3 in location 2. The subsurface resistivity along this section ranges from about 7 to 367 Ωm and a depth of about 1.38 m was investigated. The 2D electrical resistivity section can be characterized into three main geoelectric layers based on its vertical and lateral variation in electrical resistivity values.

The first region is with resistivity range of 7 to 96.7Ωm and delineated to a depth range of 0.1 to 0.22m. The region comprises of the topsoil, the visibly oil/diesel contaminated region and humus/water wet surface region. The relatively low resistivity signatures within this region can be partly due to water-wet surfaces after precipitation or biogenically degraded surficial oil/diesel waste.

The second geoelectric layer is with relatively high electrical resistivity range of 86 to 367 Ωm which is expressive of oil/diesel waste and delineated to a depth range of 0.34 m to 0.69 m at the time of investigation. This region constitutes the suspected subsoil region that has been contaminated by the oil/diesel waste and may therefore require mitigation measures to avoid further percolation of oil/diesel waste.

The third geoelectric layer is with electrical resistivity range of 53 to 140 Ωm which can be associated to the lateritic soil and delineated to an average depth of about 1.38m.

4.2.4.4 Traverse 4

Figure 4.14b represents the interpreted inverted 2D electrical resistivity section along Traverse 4 in location 2. The subsurface resistivity along this section ranges from about 8 to 260 Ωm and a depth of about 1.38 m was investigated. The 2D electrical resistivity section can be characterized

into four main geoelectric layers based on its vertical and lateral variation in electrical resistivity values.

The first region is with resistivity range of 8 to 46 Ωm and delineated to a depth range of 0.1 to 0.15 m. The region comprises of the topsoil, the visibly oil/diesel contaminated region and humus/water wet surface region. The relatively low resistivity signatures within this region can be partly due to water-wet surfaces after precipitation or biogenically degraded surficial oil/diesel waste.

The second geoelectric layer is with relatively high electrical resistivity range of 110 to 260 Ωm which is expressive of oil/diesel waste and delineated to a depth range of 0.1 m to 0.4 m at the

time of investigation. This region constitutes the suspected subsoil region that has been contaminated by the oil/diesel waste and may therefore require mitigation measures to avoid further percolation of oil/diesel waste.

The third geoelectric layer is with electrical resistivity range of 19 to 46 Ωm which can be associated to the lateritic soil/clayey sand and delineated to a depth range of 1 to 1.1m.

The fourth geoelectric layer is with relatively high electrical resistivity range of 71 to 110 Ωm and average depth of about 1.38m.

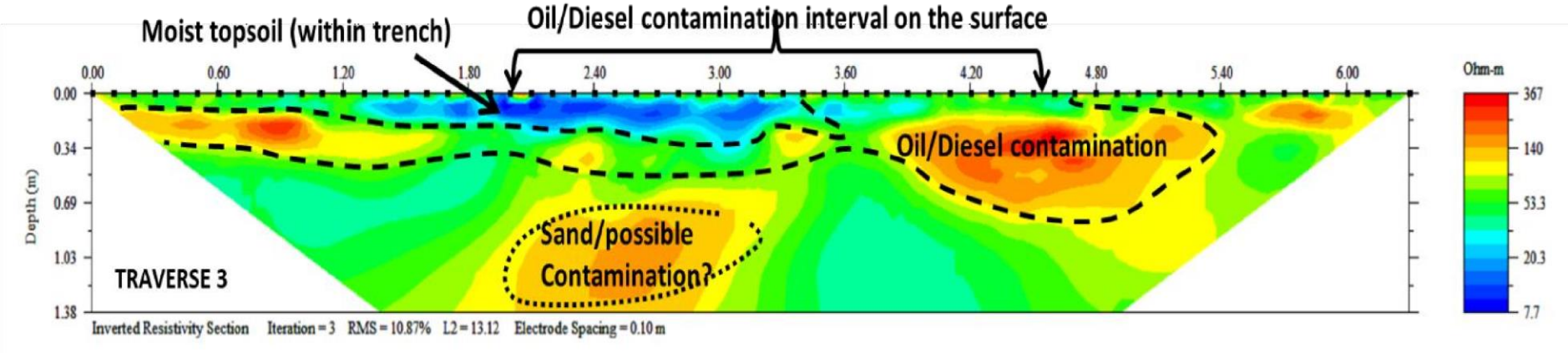

Figure 4.14a. Interpreted 2D inverted resistivity section on Traverse 3

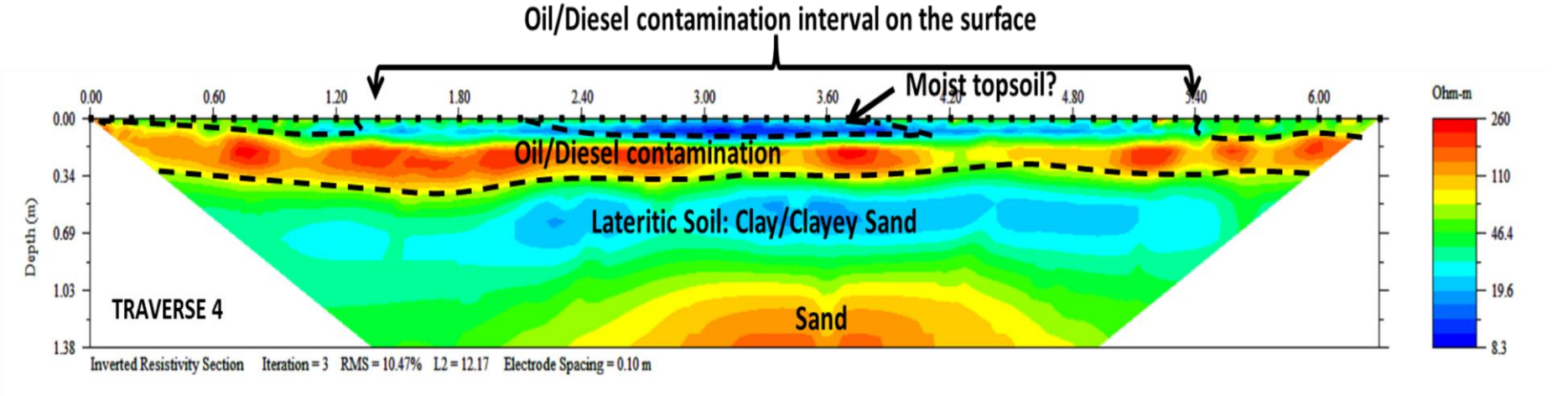

Figure 4.14b. Interpreted 2D inverted resistivity section on Traverse 4

4.2.4.5 Traverse 5A

Figure 4.15a represents the interpreted inverted 2D electrical resistivity section along Traverse 5A in location 2. The subsurface resistivity along this section ranges from about 6 to 959 Ωm and a depth of about 1.38 m was investigated. The 2D electrical resistivity section can be characterized into three main geoelectric layers based on its vertical and lateral variation in electrical resistivity values.

The first region is with resistivity range of 8 to 47 Ωm and delineated to a depth range of 0.1 to 0.8 m. The region comprises of the topsoil, the visibly oil/diesel contaminated region and humus/water wet surface region. The relatively low resistivity signatures within this region can be partly due to water-wet surfaces after precipitation or biogenically degraded surficial oil/diesel waste.

The second geoelectric layer is with relatively high electrical resistivity range of 140 to 959 Ωm which is expressive of oil/diesel waste and delineated to a depth range of 0.2 m to 0.5 m at the time of investigation. This region constitutes the suspected subsoil region that has been contaminated by the oil/diesel waste and may therefore require mitigation measures to avoid further percolation of oil/diesel waste.

The third geoelectric layer is with electrical resistivity range of 20 to 74 Ωm which can be associated to the lateritic soil/clayey sand and delineated to an average depth of about 1.38m.

4.2.4.6 Traverse 5B

Figure 4.15b represents the interpreted inverted 2D electrical resistivity section along Traverse 5B in location 2. The subsurface resistivity along this section ranges from about 5 to 950 Ωm and a depth of about 1.38 m was investigated. The 2D electrical resistivity section can be characterized

into three main geoelectric layers based on its vertical and lateral variation in electrical resistivity values.

The first region is with resistivity range of 5 to 43 Ωm and delineated to a depth range of 0.1 to 0.15 m. The region comprises of the topsoil, the visibly oil/diesel contaminated region and humus/water wet surface region. The relatively low resistivity signatures within this region can be partly due to water-wet surfaces after precipitation or biogenically degraded surficial oil/diesel waste.

The second geoelectric layer is with relatively high electrical resistivity range of 131 to 950 Ωm which is expressive of oil/diesel waste and delineated to a depth range of 0.3 m to 0.5 m at the time of investigation. This region constitutes the suspected subsoil region that has been contaminated by the oil/diesel waste and may therefore require mitigation measures to avoid further percolation of oil/diesel waste.

The third geoelectric layer is with electrical resistivity range of 18 to 68 Ωm which can be associated to the lateritic soil/clayey sand and delineated to an average depth of about 1.38m.

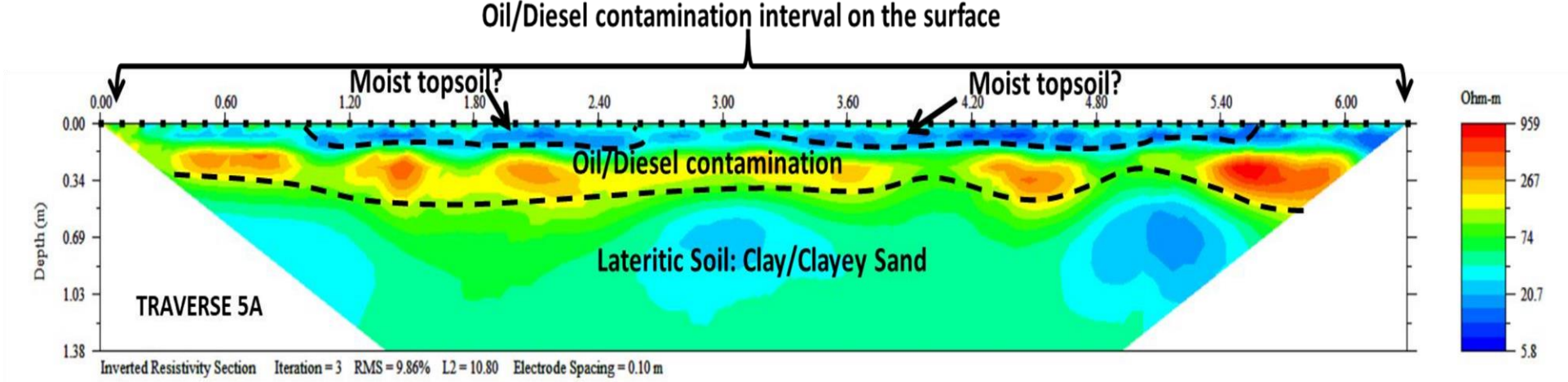

Figure 4.15a. Interpreted 2D inverted resistivity section on Traverse 5a

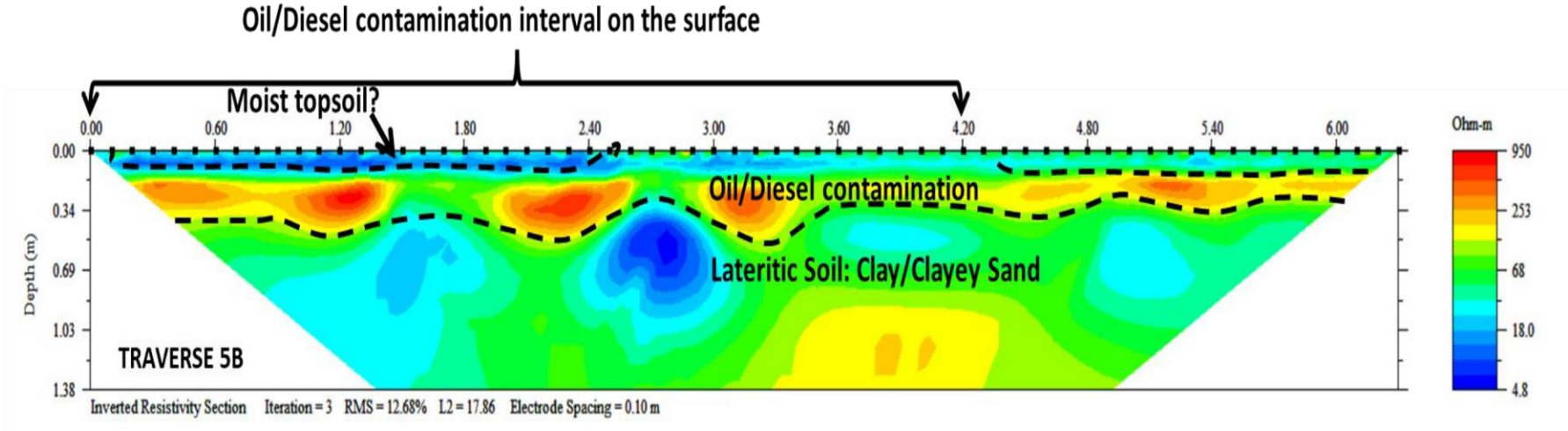

Figure 4.15b. Interpreted 2D inverted resistivity section on Traverse 5b

4.2.4.7 Traverse 6A

Figure 4.16a represents the interpreted inverted 2D electrical resistivity section along Traverse 6A in location 2. The subsurface resistivity along this section ranges from about 7 to 3815Ωm and a depth of about 1.38 m was investigated. The 2D electrical resistivity section can be characterized into four main geoelectric layers based on its vertical and lateral variation in electrical resistivity values.

The first region is with resistivity range of 6 to 33 Ωm and delineated to a depth range of 0.1 to 0.18 m. This region comprises of the topsoil, the visibly oil/diesel contaminated region and humus/water wet surface region. The relatively low resistivity signatures within this region can be partly due to water-wet surfaces after precipitation or biogenically degraded surficial oil/diesel waste.

The second geoelectric layer is with relatively high electrical resistivity range of 162 to 3815 Ωm which is indicative of oil/diesel waste and delineated to a depth range of 0.1 m to 0.4 m at the time of investigation. This region constitutes the suspected subsoil region that has been contaminated by the oil/diesel waste and may therefore require mitigation measures to avoid further percolation of oil/diesel waste.

The third geoelectric layer is with electrical resistivity range of 33 to 73 Ωm which can be associated to the lateritic soil, clay and clayey sand and delineated to a depth range of about 1 to 1.1m.

The fourth geoelectric layer is with resistivity of about 162 Ωm which is descriptive of Sand and delineated to an average depth of about 1.38m.

4.2.4.8 Traverse 6B

Figure 4.16b represents the interpreted inverted 2D electrical resistivity section along Traverse 6B in location 2. The subsurface resistivity along this section ranges from about 5 to 2248 Ωm and a depth of about 1.38 m was investigated. The 2D electrical resistivity section can be characterized into four main geoelectric layers based on its vertical and lateral variation in electrical resistivity values.

The first region is with resistivity range of 5 to 22 Ωm and delineated to a depth range of 0.1 to 0.2 m. The region comprises of the topsoil, the visibly oil/diesel contaminated region and humus/water wet surface region. The relatively low resistivity signatures within this region can

be partly due to water-wet surfaces after precipitation or biogenically degraded surficial oil/diesel waste.

The second geoelectric layer is with relatively high electrical resistivity range of 296 to 2248 Ωm which is expressive of oil/diesel waste and delineated to a depth range of 0.17 m to 0.4 m at the time of investigation. This region constitutes the suspected subsoil region that has been contaminated by the oil/diesel waste and may therefore require mitigation measures to avoid further percolation of oil/diesel waste.

The third geoelectric layer is with electrical resistivity range of 22 to 105 Ωm which can be associated to the lateritic soil, clay and clayey sand and delineated to a depth range of about 1 to 1.1m.

The fourth geoelectric layer is with resistivity of about 105 Ωm which is descriptive of Sand and delineated to an average depth of about 1.38m.

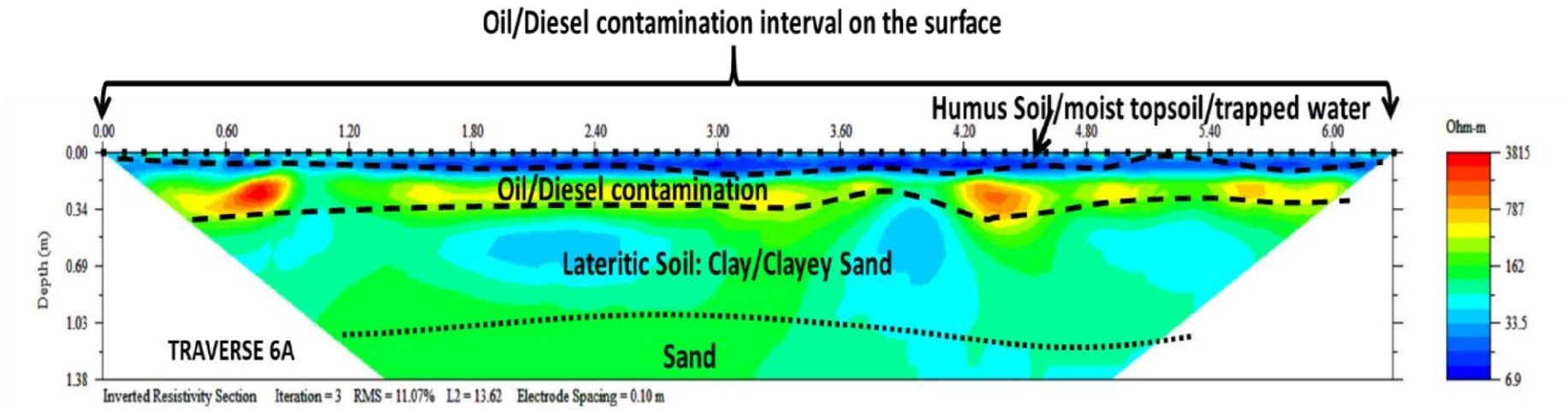

Figure 4.16a. Interpreted 2D inverted resistivity section on Line 6a

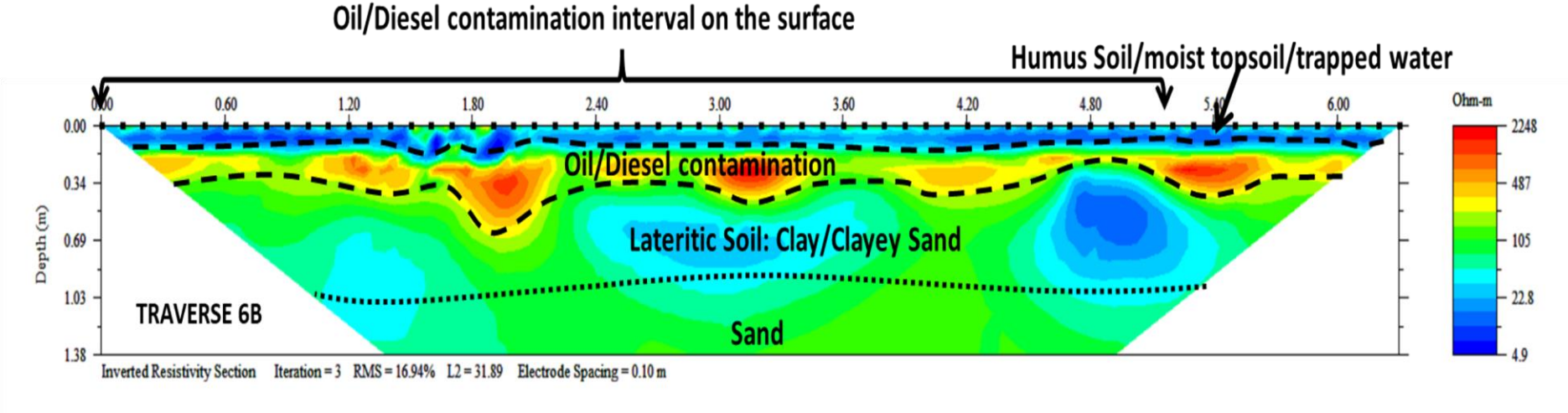

Figure 4.16b Interpreted 2D inverted resistivity section on Line 6b

4.2.4.9 Traverse 7A

Figure 4.17a represents the interpreted inverted 2D electrical resistivity section along Traverse 7A in location 2. The subsurface resistivity along this section ranges from about 5 to 868 Ωm and a depth of about 1.38 m was investigated. The 2D electrical resistivity section can be characterized into four main geoelectric layers based on its vertical and lateral variation in electrical resistivity values.

The first region is with resistivity range of 5 to 65 Ωm and delineated to a depth range of 0.1 to 0.16. This region comprises of the topsoil, the visibly oil/diesel contaminated region and humus/water wet surface region. The relatively low resistivity signatures within this region can be partly due to water-wet surfaces after precipitation or biogenically degraded surficial oil/diesel waste.

The second geoelectric layer is with relatively high electrical resistivity range of 151 to 868Ωm which can be indicative of oil/diesel waste and delineated to a depth range of 0.3 m to 0.4 m at the time of investigation.

The third geoelectric layer is with electrical resistivity range of 34 to 65 Ωm which can be associated to the lateritic soil, clay and clayey sand and delineated to a depth range of about 1 to 1.2m.

The fourth geoelectric layer is with resistivity range of about 124 to 238 Ωm which is descriptive of Sand and delineated to an average depth of about 1.38 m.

4.2.4.10 Traverse 7B

Figure 4.17b represents the interpreted inverted 2D electrical resistivity section along Traverse 7B in location 2. The subsurface resistivity along this section ranges from about 6 to 803Ωm and a depth of about 1.38 m was investigated. The 2D electrical resistivity section can be characterized into four main geoelectric layers based on its vertical and lateral variation in electrical resistivity values.

The first region is with resistivity range of 6 to 22 Ωm and delineated to a depth range of 0.1 to 0.12. This region comprises of the topsoil, the visibly oil/diesel contaminated region and humus/water wet surface region.

The second geoelectric layer is with relatively high electrical resistivity range of 131 to 803 Ωm which is expressive of oil/diesel waste and delineated to a depth range of 0.3 m to 0.36 m at the time of investigation. This region constitutes the suspected subsoil region that has been contaminated by the oil/diesel waste.

The third geoelectric layer is with electrical resistivity range of 22 to 72 Ωm which can be associated to the lateritic soil, clay and clayey sand and delineated to a depth range of about 0.9 to 1.1m.

The fourth geoelectric layer is with resistivity range of about 72 to 131 Ωm which is descriptive of Sand and delineated to an average depth of about 1.38m.

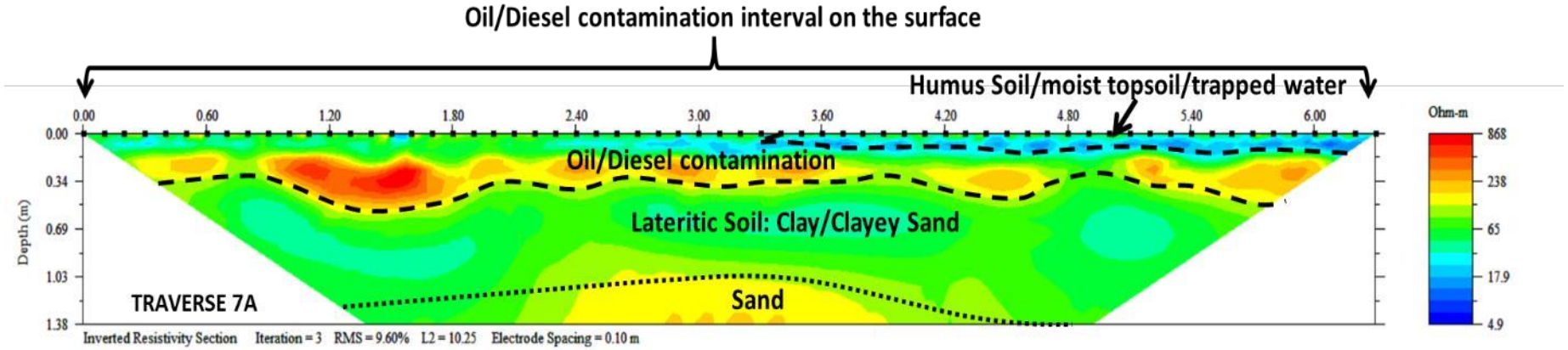

Figure 4.17a. Interpreted 2D inverted resistivity section on Line 7a

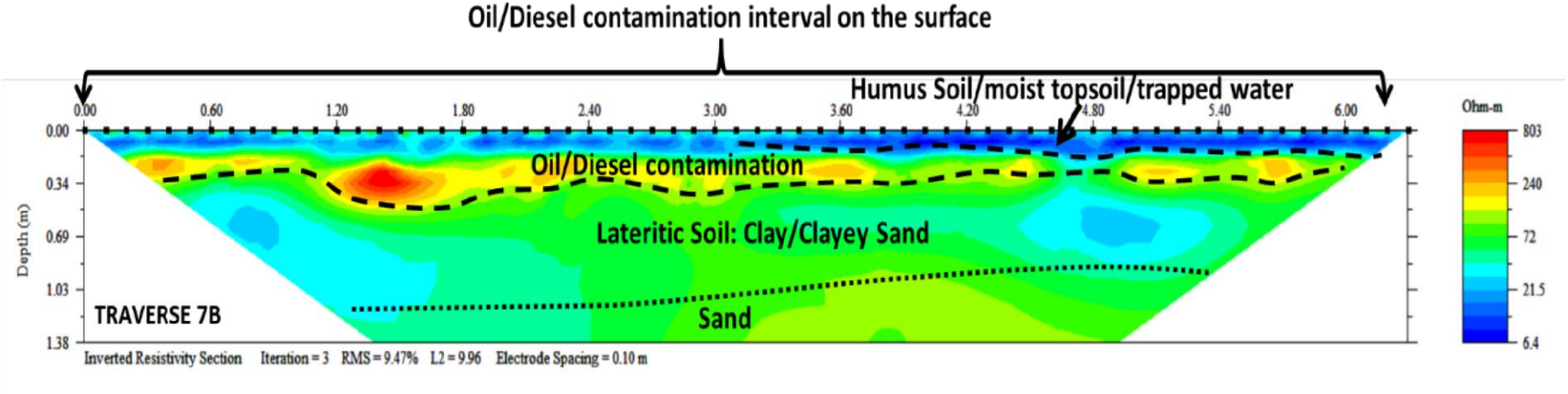

Figure 4.17b. Interpreted 2D inverted resistivity section on Line 7b

4.2.4.11 Traverse 8

Figure 4.18 represents the interpreted inverted 2D electrical resistivity section along Traverse 8 in location 2. This traverse is along the slope of the area and the vertical scale is the elevation above sea level after elevation correction The subsurface resistivity along this section ranges from about 2 to 13,161 Ωm and a depth of about 1.38 m was investigated. The 2D electrical resistivity section can be characterized into three main geoelectric layers based on its vertical and lateral variation in electrical resistivity values.

The first region is with resistivity range of 2 to 19 Ωm and delineated to a depth range of 0.1 to 0.2 m. This region comprises of the topsoil, the visibly oil/diesel contaminated region and humus/water wet surface region. The relatively low resistivity signatures within this region can be partly due to water-wet surfaces after precipitation or biogenically degraded surficial oil/diesel waste. The elevation correction has properly positioned the diesel contamination zones and it can be observed that the preferential accumulation of the contaminants may be influenced by variation in topography.

The second geoelectric layer is with relatively high electrical resistivity range of 168 to 13,161 Ωm which is expressive of oil/diesel waste and delineated to a depth range of 0.4 m to 0.85 m at the time of investigation. This region constitutes the suspected subsoil region that has been contaminated by the oil/diesel waste.

The third geoelectric layer is with electrical resistivity range of 19 to 168 Ωm which can be associated to the lateritic soil, clay and clayey sand and delineated to an average depth of about

1.38m.

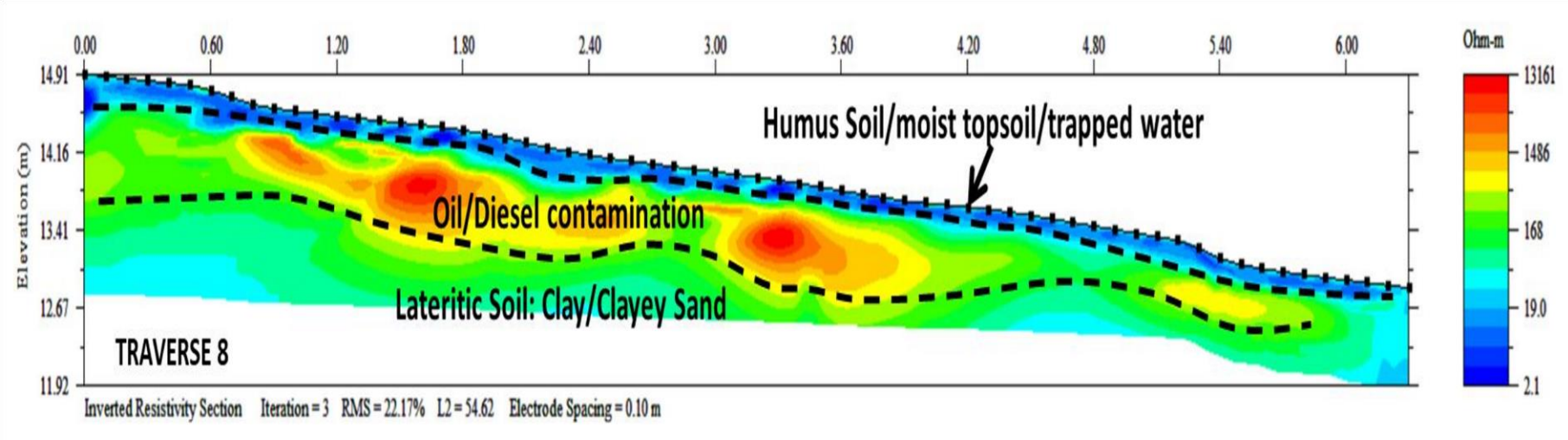

Figure 4.18. Interpreted (elevation corrected) 2D inverted resistivity section on Line 8

4.2.5 DISCUSSION OF GPR RESULTS IN LOCATION 2

The 2D radargrams in this discussion have been presented in coloured format (Red-Green-Blue) for enhanced visualisation of amplitude attenuation.

4.2.5.1 Discussion of Traverse 1 GPR Radargram

The interpreted 2D radargram for Traverse 1 in Location 2 is presented in Figure 4.19. The first reflection observed on the radargram is the ground surface/topsoil and arises due to the relative permittivity variation between air and ground surface. This region is underlain by attenuated or low amplitude reflection which is suggestive of the presence of oil/diesel polluted subsurface region and has been mapped to a depth range of 0.7 to 0.9 m. The third region is with high amplitude event which can be attributed to lateritic soil and delineated to a depth of about 2 m.

Beyond this region, the radargram is represented by low amplitude event which is suggestive of Clay layer.

4.2.5.2 Discussion of Traverse 2 GPR Radargram

The interpreted 2D radargram for Traverse 2 in Location 2 is presented in Figure 4.20. The first reflection observed on the radargram is the ground surface/topsoil and arises due to the relative permittivity variation between air and ground surface. This region is underlain by attenuated or low amplitude reflection which is suggestive of the presence of oil/diesel polluted subsurface region and has been mapped to a depth range of 0.5 to 0.8m. The third region is with high amplitude event which can be attributed to lateritic soil and delineated to a depth of about 2.5m. Beyond this region, the radargram is represented by low amplitude event which is suggestive of Clay layer.

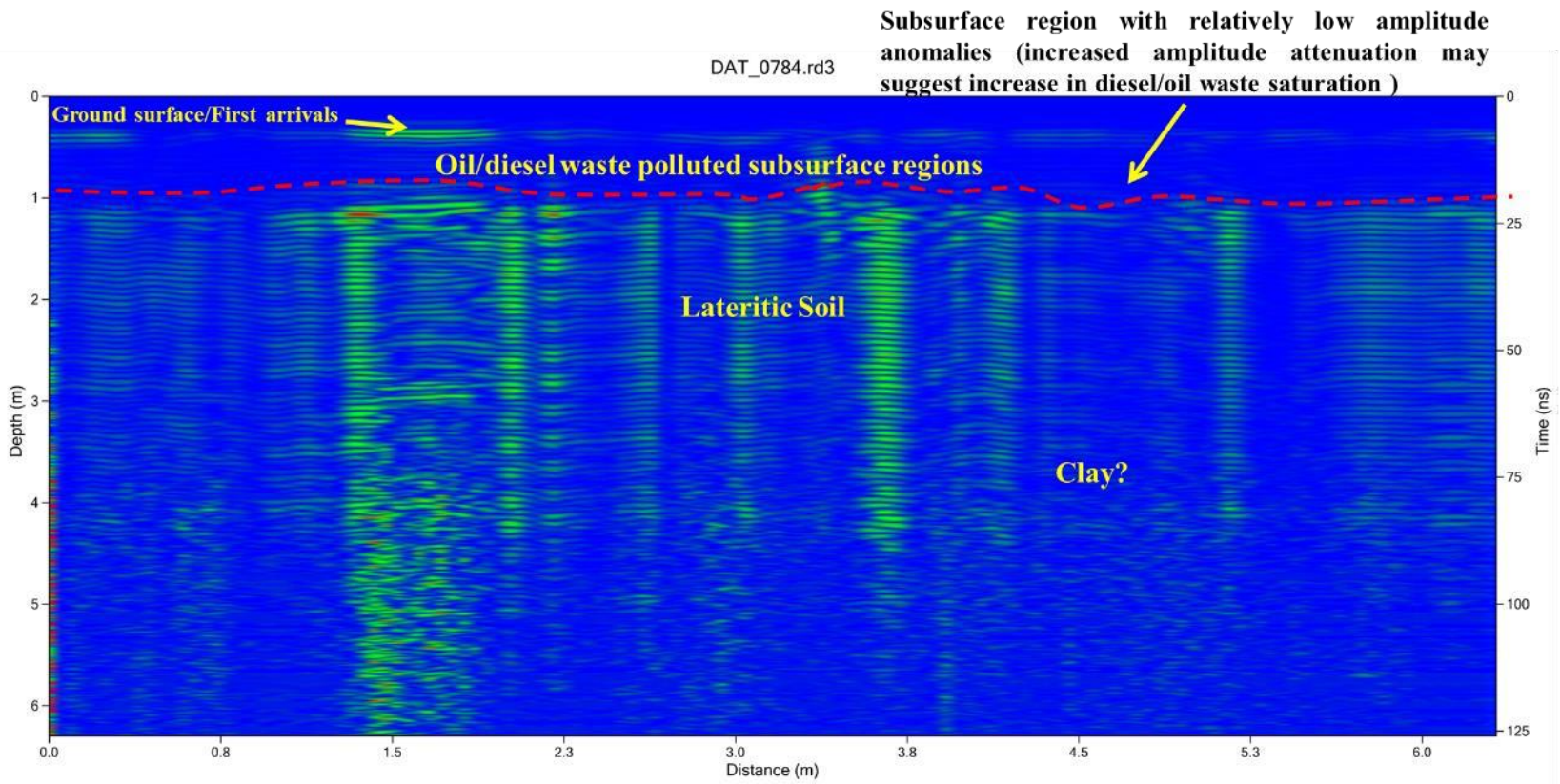

Figure 4.19 Interpreted GPR radargram using the 450 MHz antenna along Traverse 1 at Location 2

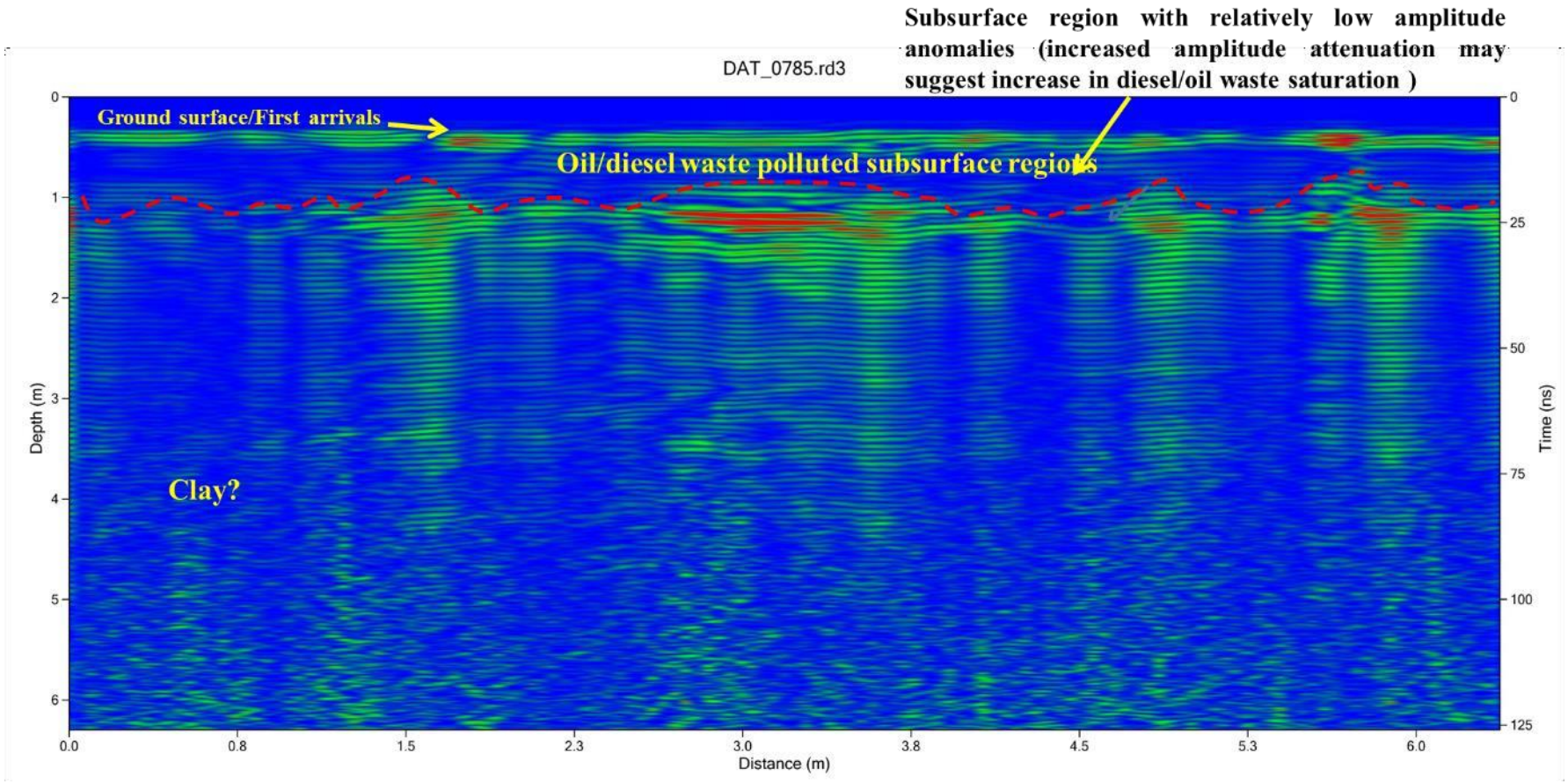

Figure 4.20 Interpreted GPR radargram using the 450 MHz antenna along Traverse 2 at Location 2

4.2.5.3 Discussion of Traverse 3 GPR Radargram

The interpreted 2D radargram for Traverse 3 in Location 2 is presented in Figure 4.21. The first reflection observed on the radargram is the ground surface/topsoil and arises due to the relative permittivity variation between air and ground surface. This region is underlain by attenuated or low amplitude reflection which is suggestive of the presence of oil/diesel polluted subsurface region and has been mapped to a depth range of 0.7 to 0.9 m. The third region is with high amplitude event which can be attributed to lateritic soil and delineated to a depth of about 2 m.

Beyond this region, the radargram is represented by low amplitude event which is suggestive of Clay layer.

4.2.5.4 Discussion of Traverse 4 GPR Radargram

The interpreted 2D radargram for Traverse 4 in Location 2 is presented in Figure 4.22. The first reflection observed on the radargram is the ground surface/topsoil. This region is underlain by attenuated or low amplitude reflection within the lateral distance of about 1 to 6 m which is suggestive of the presence of oil/diesel polluted subsurface region and has been mapped to a depth range of 0.5 to 0.8 m. The third region is with high amplitude event which can be attributed to lateritic soil and delineated to a depth of about 2 m. Beyond this region, the radargram is represented by low amplitude event which is suggestive of Clay layer.

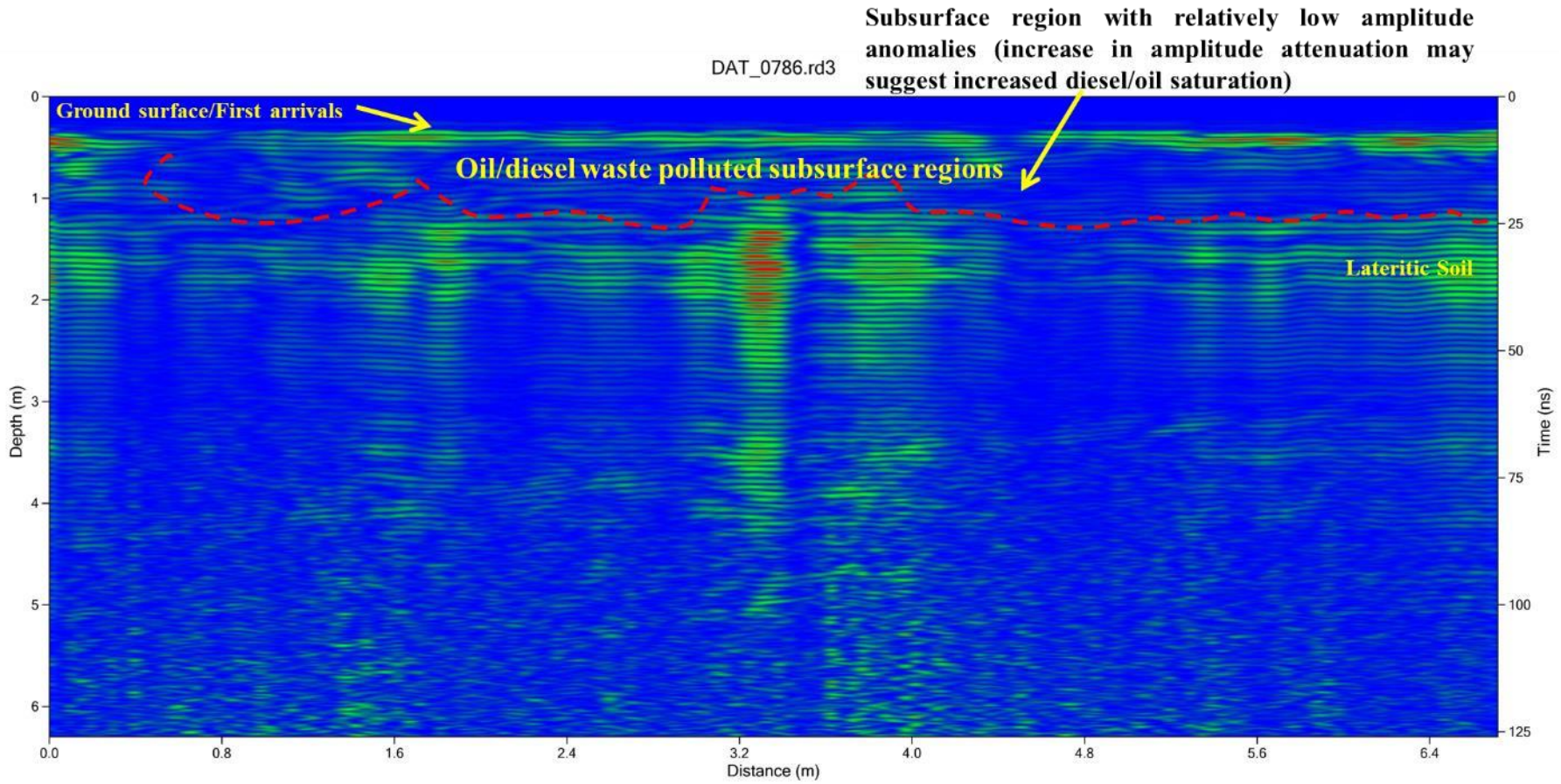

Figure 4.21 Interpreted GPR radargram using the 450 MHz antenna along traverse 3 at Location 2

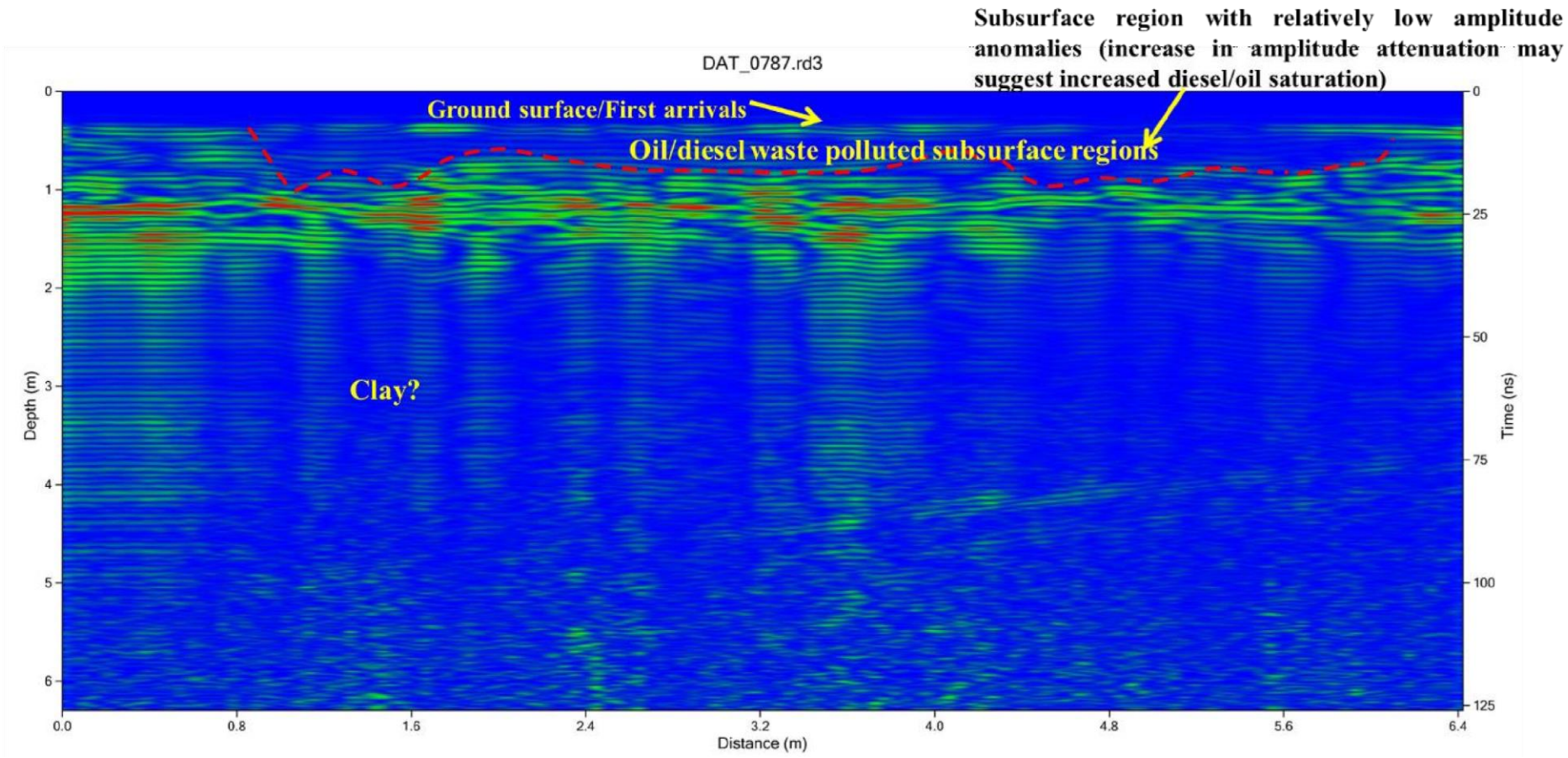

Figure 4.22 Interpreted GPR radargram using the 450 MHz antenna along traverse 4 at Location 2

4.2.5.5 Discussion of Traverse 5 GPR Radargram

The interpreted 2D radargram for Traverse 5 in Location 2 is presented in Figure 4.23. The first reflection observed on the radargram is the ground surface/topsoil and arises due to the relative permittivity variation between air and ground surface. Within the lateral distance of 4 to 9m and depth range of 0.6 to 1 m, attenuated or low amplitude reflection is prevalent. This is suggestive of the presence of oil/diesel polluted subsurface region. The third region is with high amplitude event which can be attributed to lateritic soil and delineated to a depth of about 2 m. Beyond this region, the radargram is represented by low amplitude event which is suggestive of Clay layer.

4.2.5.6 Discussion of Traverse 6 GPR Radargram

The interpreted 2D radargram for Traverse 6 in Location 2 is presented in Figure 4.24. The first reflection observed on the radargram is the ground surface/topsoil and arises due to the relative permittivity variation between air and ground surface. Within the lateral distances of 0 to 3.5 and 5 to 11m, attenuated or low amplitude reflection can be observed which is suggestive of the presence of oil/diesel polluted subsurface region and has been mapped to a depth range of 0.5 to 0.7 m. The third region is with high amplitude event which can be attributed to lateritic soil/sand and delineated to a depth of about 2m. Beyond this region, the radargram is represented by low amplitude event which is suggestive of Clay layer.

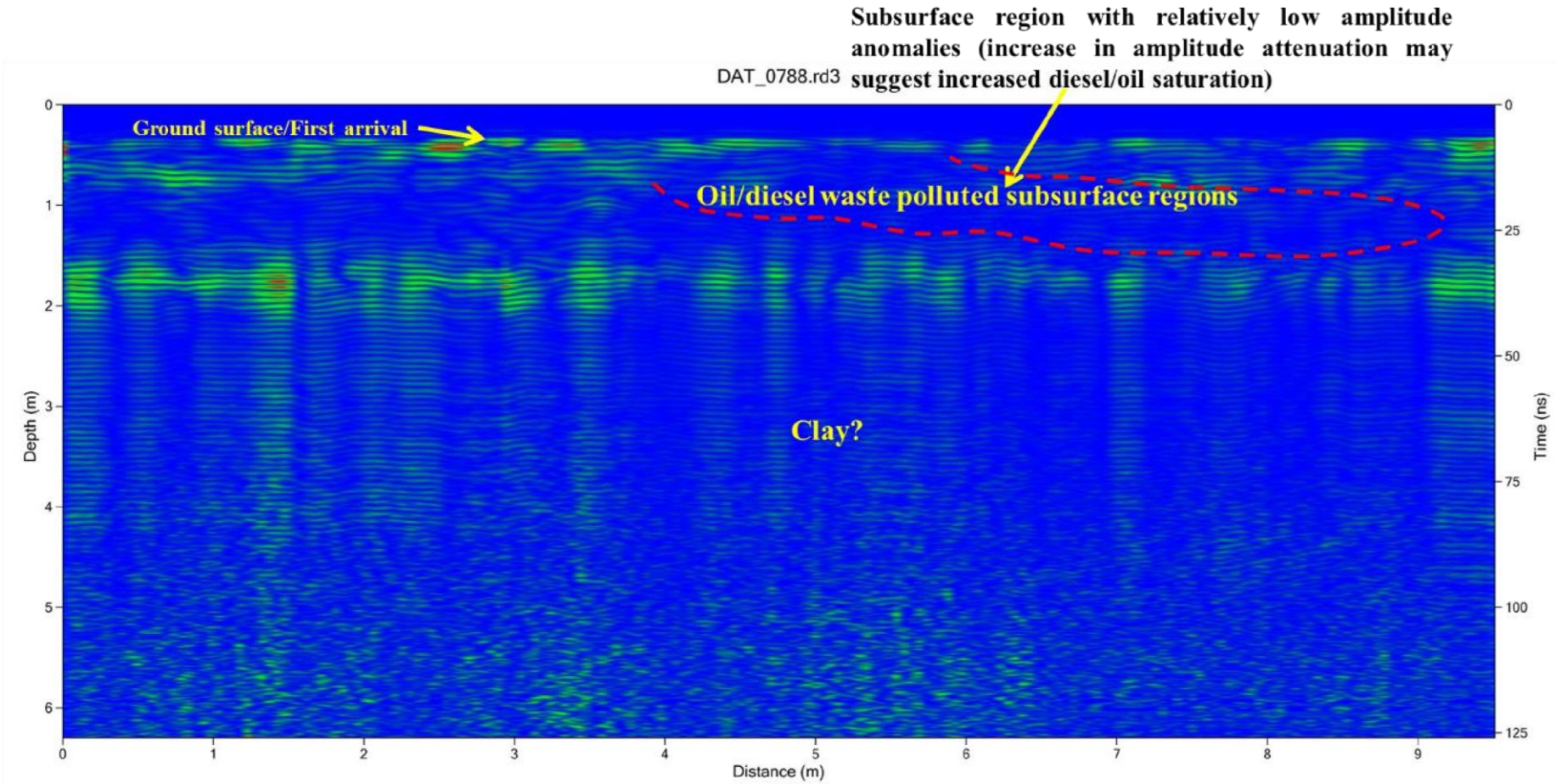

Figure 4.23 Interpreted GPR radargram using the 450 MHz antenna along traverse 5 at Location 2

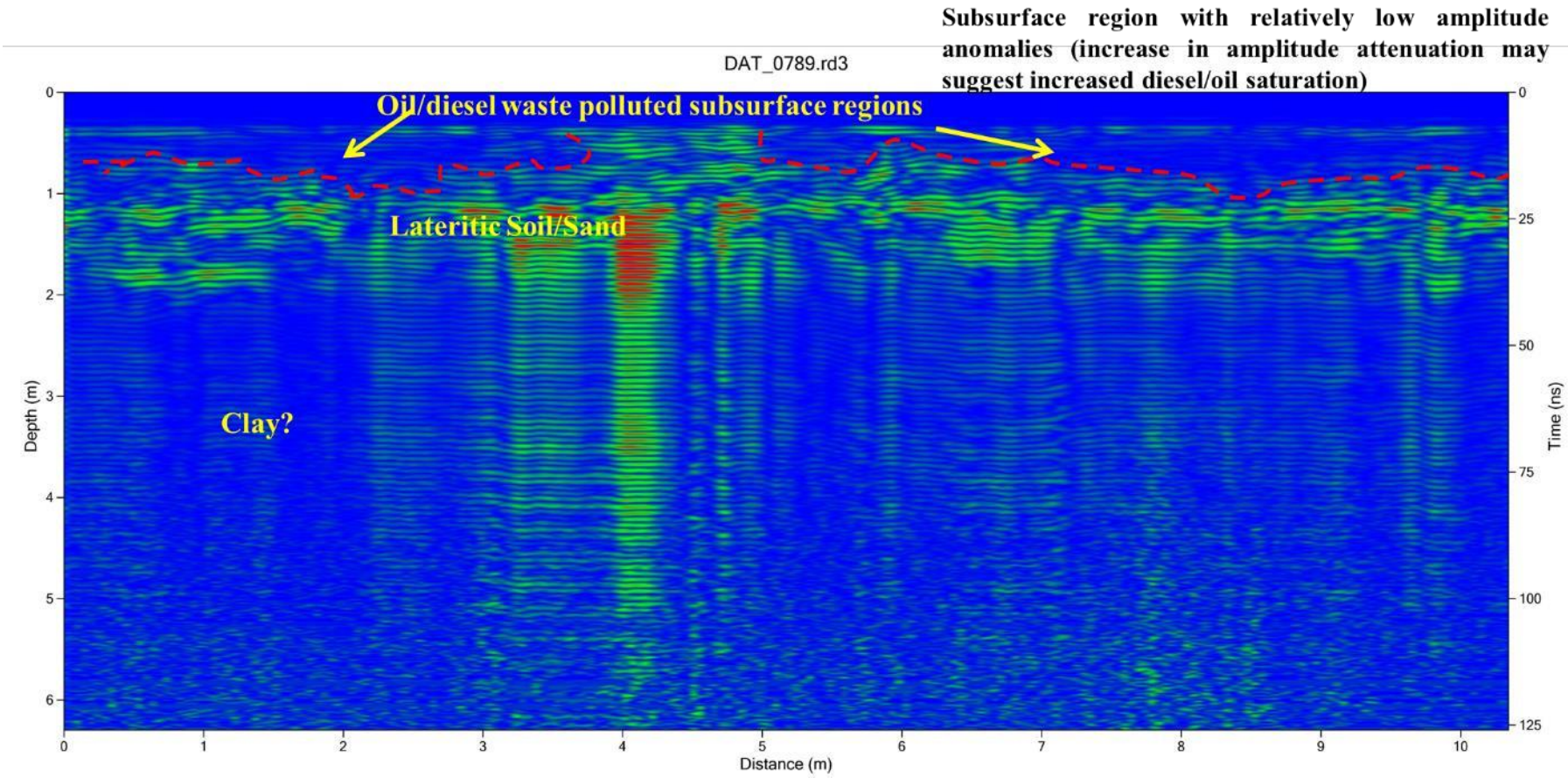

Figure 4.24 Interpreted GPR radargram using the 450 MHz antenna along traverse 6 at Location 2

4.2.5.7 Discussion of Traverse 7 GPR Radargram

The interpreted 2D radargram for Traverse 7 in Location 2 is presented in Figure 4.25. The first reflection observed on the radargram is the ground surface/topsoil and arises due to the relative permittivity variation between air and ground surface. Within the lateral distances of 0 to 5 and 6 to 10 m, attenuated or low amplitude reflection can be observed which is suggestive of the presence of oil/diesel polluted subsurface region and has been mapped to a depth range of 0.6 to 1 m. The third region is with high amplitude event which can be attributed to lateritic soil/sand and delineated to a depth of about 2.2m. Beyond this region, the radargram is represented by low amplitude event which is suggestive of Clay layer.

4.2.5.8 Discussion of Traverse 8 GPR Radargram

The interpreted 2D radargram for Traverse 8 in Location 2 is presented in Figure 4.26. The first reflection observed on the radargram is the ground surface/topsoil and arises due to the relative permittivity variation between air and ground surface. This region is underlain by attenuated or low amplitude reflection which is more prevalent within the lateral of 0 to about 18m, beyond this region the attenuation is minimal. The degree of amplitude attenuation is therefore suggestive of the saturation of the oil/diesel polluted subsurface region as it can be observed that regions that are proximal to the source are more attenuated than regions farther away from the source of oil/diesel waste pollution. The pollutants have been mapped to a depth range of 0.7 to 1

m. The third region is with high amplitude event which can be attributed to lateritic soil/sand and delineated to a depth of about 2.2 m. Beyond this region, the radargram is represented by low amplitude event which is suggestive of Clay layer.

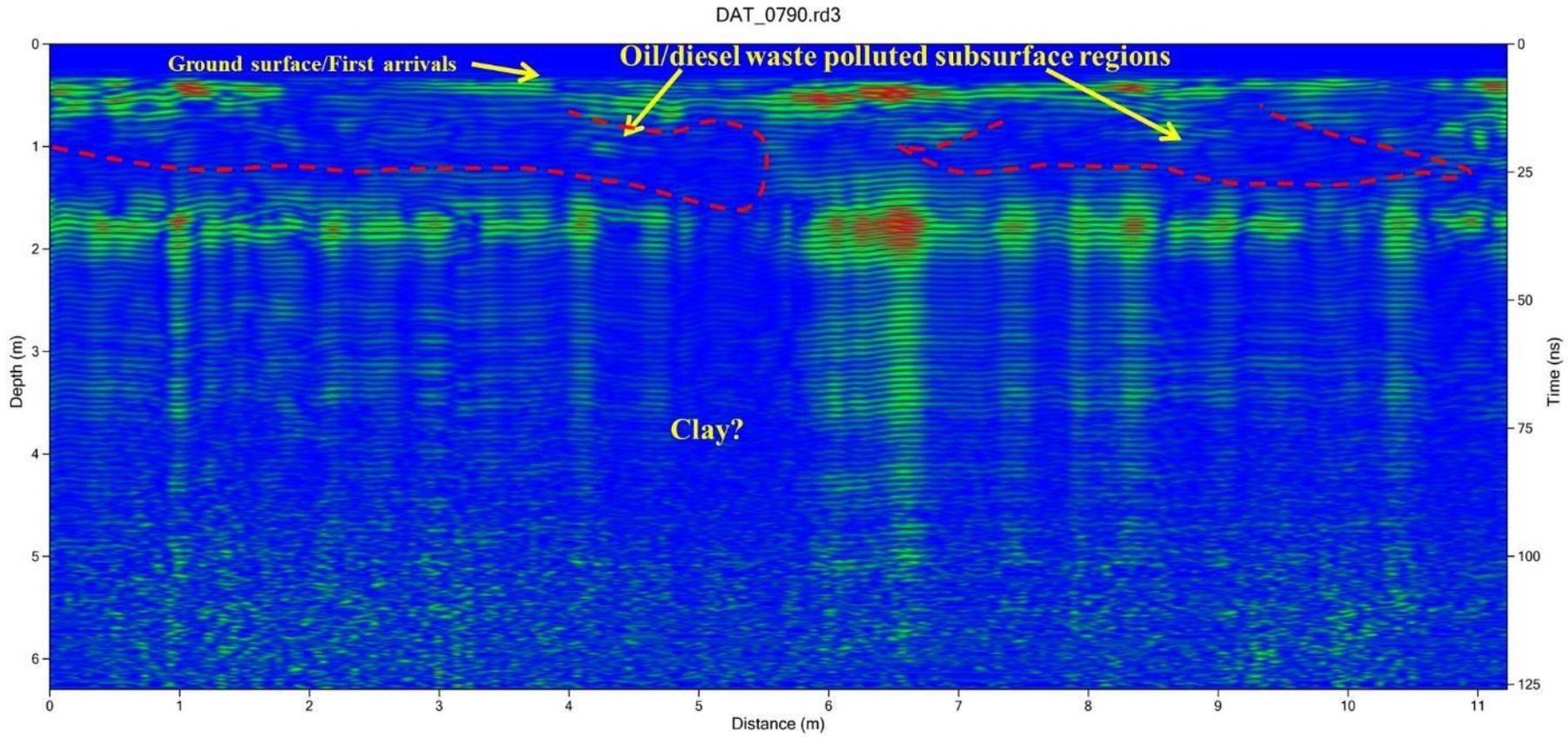

Figure 4.25 Interpreted GPR radargram using the 450 MHz antenna along traverse 7 at Location 2

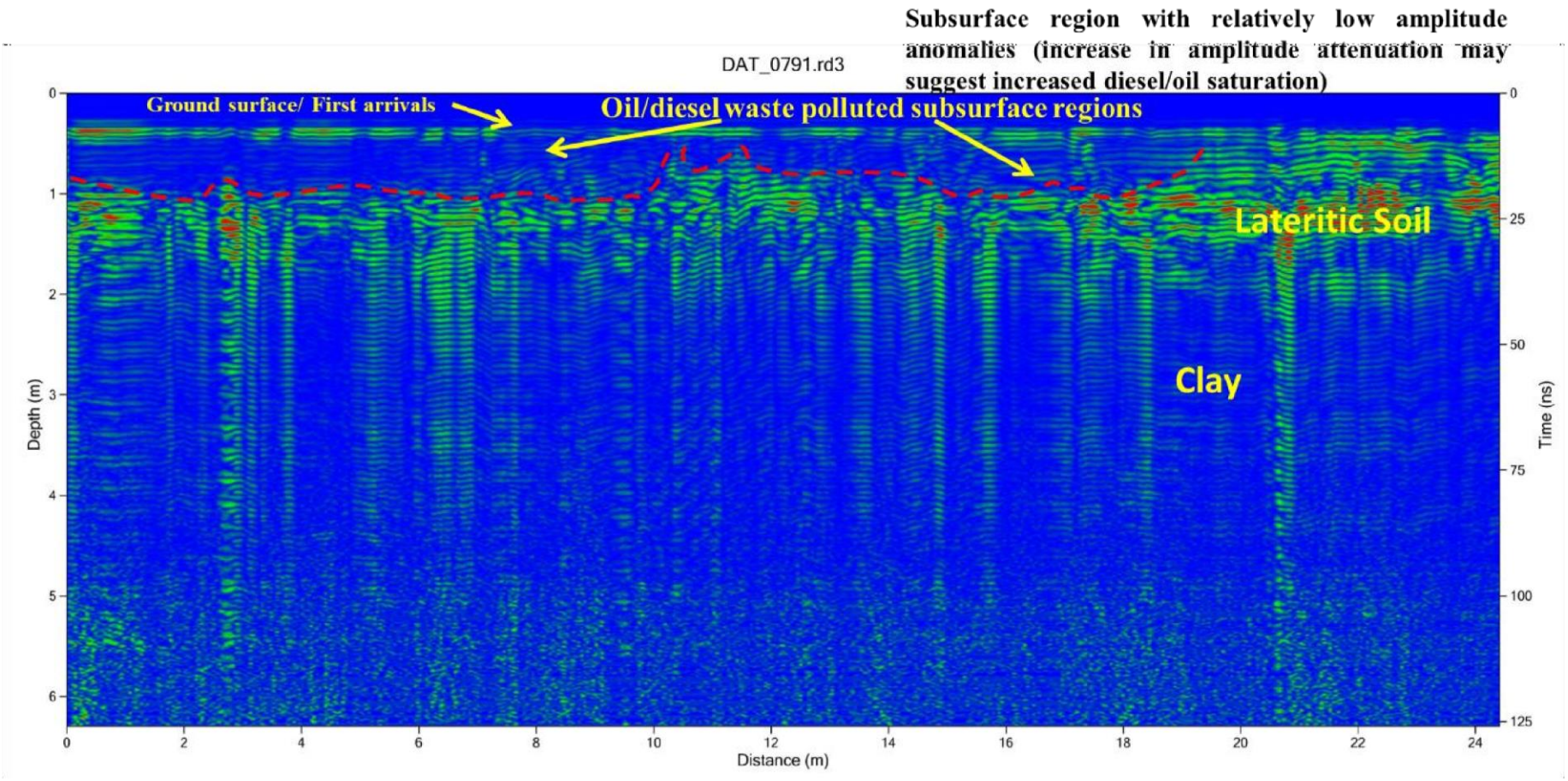

Figure 4.26 Interpreted GPR radargram using the 450 MHz antenna along traverse 8 middle line at Location 2

CHAPTER FIVE

CONCLUSION AND RECOMMENDATIONS

5.1 CONCLUSION

Geophysical investigation involving Electrical Resistivity (2D ERT) and GPR methods were deployed at two locations within MTU Campus, Ibafo, Southwestern Nigeria to investigate wastewater seepage and diesel/oil discharge respectively. The first location involves waste-water seepage from pipes and underground tank while the second site is a prolonged diesel/oil discharge from a diesel-powered generating plant within the campus.

The result has shown that the waste-water seepage is represented by low resistivity range of 1 to 29 Ωm within the depth range of 0.9 to 3.5 on the 2D ERT technique. The high resolution (0.2 m minimum electrode spacing) 2D ERT has mapped the position of a pipe as a low resistivity circular structure at a depth of 0.5 m. This pipe is suspected to be leaking and should be one of the sources of the seepage water. The observed surface seepage and the subsurface low resistivity region has been mapped uphill of the pipe position which implies that the walls of the underground concrete storage might be compromised and seepage must have also occurred from its walls. The 3D inverted resistivity cube from the parallel 2D ERT lines have shown the distribution of the low resistivity on the surface which is consistent with the observed surface seepage. Dynamic slices and 3D Isoresistivity surface contour plots have shown that the low resistivity region is extensive at depths of about 1m and implies that the seepage has spread beyond surface observations. Beneath, the polluted region, the subsurface is characterised by electrical resistivity range of 18 to 72 Ωm and 102 to 268 Ωm which is expressive of lateritic soil and Sand layers respectively.

Similarly, the GPR methods in location 1 has shown the position of the buried pipe and has been mapped within the depth range of 0.4 to 0.6 m. The waste water polluted region is characterised by high amplitude anomalies within the depth range of 1.2 and 2.6 m. The high amplitude anomaly can be associated to the relatively higher water saturation and energy reflection within the waste water polluted regions. Regions around the pipe has shown high amplitude anomalies compared to other regions which implies possible pipe leakage. The correlated GPR lines have shown that the amplitude anomalies reduce as one traverses away from the source of pollution.

In location 2, the subsurface is characterised to three to four layers on the 2D Electrical resistivity technique. The first geoelectric layer is with resistivity range of 2 to 19 Ωm and delineated to a depth range of 0.1 to 0.2 m. This region comprises of the topsoil, the visibly oil/diesel contaminated region and humus/water wet surface region. The relatively low resistivity signatures within this region can be partly due to water-wet surfaces after precipitation or biogenically degraded surficial oil/diesel waste. The second geoelectric layer is with relatively high electrical resistivity range of

131 to 13,161 Ωm which is expressive of oil/diesel waste and delineated to a depth range of 0.3 m to 0.85 m at the time of investigation. This region constitutes the suspected subsoil region that has been contaminated by the oil/diesel waste. The elevation correction carried out on the line (Traverse 8) taken along the slope has properly positioned the diesel contamination zones and it can be observed that the preferential accumulation of the contaminants may be influenced by variation in topography. The third geoelectric layer is with electrical resistivity range of 19 to 72 Ωm which can be associated to the lateritic soil, clay and clayey sand and delineated to a depth range of about 0.9 to 1.38 m. On some lines down the slope, the fourth geoelectric layer is

characterised by resistivity range of about 72 to 131 Ωm which is descriptive of Sand and delineated to an average depth of about 1.38m.

On the interpreted radargram for location 2, the first reflection observed on the radargram is the ground surface/topsoil and arises due to the relative permittivity variation between air and ground surface. This region is mainly underlain by attenuated or low amplitude reflection which is suggestive of the presence of oil/diesel polluted subsurface region and has been mapped to a depth range of 0.5 to 1 m. It can be observed that regions that are proximal to the source of the oil/diesel waste are more attenuated than regions farther away from the source of the pollution. It can therefore be deduced that the degree of amplitude attenuation is relative to the subsurface saturation of the oil/diesel waste. The third region is with high amplitude event which can be attributed to Sand/lateritic soil and delineated to a depth of about 2 m. Beyond this region, the radargram is represented by low amplitude event which is suggestive of Clay layer.

5.2 RECOMMENDATIONS

From the result of the study, it is recommended that the integrity of the underground waste tank in location 1 should be checked as there is likelihood that the wall of the underground concrete tank might be one of the sources of the seepage. This may therefore call for renovation of the underground tank. Similarly, the mapped buried pipe is recommended for renovation as there are indications that it is leaking. For the second location, it is recommended that mitigation measures should be put in place to control or collect the oil/diesel waste discharge from the generator. Furthermore, the electrical resistivity and GPR methods are recommended as an effective tool for mapping of contaminants plume in oil pollution sites such as parts of the Ogoni land, Niger Delta and other regions with septic or oil pollutions.

REFERENCES

Abdullah M. Al-Amri. (2018) Dept. of Geology & Geophysics King Saud University, Riyadh, Applied Geophysics

Adam, G., Gamoh, K., Morris, D. G., and Duncan, H (2002), Effects of alcohol addition on the movement of petroleum hydrocarbon fuels in soil. Science of the Total Environment, 286 (1/3), 15-25

Adebiyi, A.O, (2014), Lithostratigraphy, Palynostratigraphy and Palynofacies Indications of the Depositional Environments of Upper Cretaceous to Paleogene Sediments, Offshore Eastern Dahomey Basin, SW Nigeria. Journal of Earth Science Research, 2, 118-128

Adebiyi, A.O, (2015), Upper Cretaceous to Paleogene Palynosequence Stratigraphy of H-1 Well Offshore Eastern Dahomey Basin, Southwestern Nigeria. International Journal of Research and Innovations in Earth Science (IJRIES), 2, 82-88

Adeigbe, O.C., Ola-Buraimo, A.O., Moronhunkola, A.O, (2013), Palynological Characterization of the Tertiary Offshore Emi-1 Well, Dahomey Basin, Southwestern Nigeria. International Journal of Scientific & Technology Research (IJSTR), 2, 58-70

Billman, H.G, (1978), Offshore Stratigraphy and paleontology of the Dahomey Embayment, West Africa. Proceeding in 7th African Micropaleontological Colloquium Ile-lfe (Nigeria), 21-46

Billman, H.G. (1992), Offshore Stratigraphy and Paleontology of the Dahomey Embayment, West Africa. Nigerian Association Petroleum Explorationists, 7, 121-130

Botterill, A (2020). Ground Penetrating Radar Limitations.https://www.Mantraservices.co.uk. Retrieved on 27th February

Cheng, Y., and Nathanial, P.C. (2009), Generic assessment criteria for human health risk assessment of potentially contaminated land in China, Science of the Total Environment, 408(2), 324-339

Dakhnov, V.N., (1962), Geophysical Well logging. Q. Colorado Sch. Mines. 57 – 2,445

Loke M.H. (2000), Electrical imaging surveys for environmental and engineering studies

Flóvenz, Ó.G., Georgsson, L.S., and Árnason, K., (1985): Resistivity structure of the upper crust in Iceland, J. Geophys 10,136-10,150.

Gérard Alfred Franck d'Almeida, Christophe Kaki, James Adejimi Adeoye (2016). Benin and Western Nigeria Offshore Basins: A Stratigraphic Nomenclature Comparison, International Journal of Geosciences, 7, 177-188

Gylfi Páll Hersir and Knútur Árnason, (2010) Resistivity of Rocks, in Exploration for Geothermal Resources, Oct. 29 – Nov. 19

Hruska J, Cermák J and Sustek S. (1999). Mapping tree root systems with ground penetrating radar. Tree physiology 19: 125 - 130

Jeffrey J. Daniels a, Roger Roberts a, Mark Vendl, (1995). Ground penetrating radar for the detection of liquid contaminants, Journal of Applied Geophysics 33, pg 195-207

Jorge L. Porsani a, Walter M. Filhob, Vagner R. Elisa, Fisseha Shimeles a, Joa˜o C. Douradob, Helyelson P. Mourab (2004), The use of GPR and VES in delineating a contamination plume in a landfill site: a case study in SE Brazil, Journal of Applied Geophysics 55, 199–209

Kaki, C., d'Almeida, G.A.F., Yalo, N. and Amelina, S (2012), Geology and Petroleum Systems of the Offshore Benin Basin (Benin), Oil & Gas Science and Technology—Revue IFP Energies Nouvelles, 68, 363-381

Li Xinwu (2016) , Research On Information Clustering for Network Marketing System Based on Density-Isoline Algorithm. Acta Mechanica Malaysia, 1(1): 18-21

Martin Robinson, Charlie Bristow, Jennifer McKinley and Alastair Ruffell (2013), Ground Penetrating Radar, British society for Geomorphology, Geomorphological Techniques, Part 1, Sec. 5.5

Mellet JS (1995), Ground penetrating radar applications in engineering, environmental management, and geology. Journal of applied geophysics 33: 157-166, 1995

Miroslaw Wyszkowski, Jadwiga Wyszkowska, Agata Borowik, Natalia Kordaia (2020), Contamination of Soil with Diesel Oil, Application of Sewage Sludge and Content of Macroelements in Oats,Water Air Soil Pollution, 231-546

Mitter, E.K., Germida, J.J. and de Freitas, J.R (2021). Impact of diesel and biodiesel contamination on soil microbial community activity and structure. Sci Rep 11, 10856

Mohamed Metwaly & Mohamed Ahmed Khalil & El-Said Al-Sayed & Abeer El-Kenawy (2013), Tracing subsurface oil pollution leakage using 2D electrical resistivity tomography, Arab J Geosci 6:3527–3533

Nicholas O. Mariita (2010), schlumberger vertical soundings: techniques and interpretations with examples from kr1suv1k and glerardalur, iceland and olkaria, kenya

Nton, M.E., Ikhane, P.R. and Tijani, M.N (2009), Aspect of Rock-Eval Studies of the Maastrichtian-Eocene Sediments from Subsurface, in the Eastern Dahomey Basin Southwestern Nigeria. European Journal of Scientific Research, 25, 417-427

Omatsola, M.E. and Adegoke, O.S (1981), Tectonic Evolution and Cretaceous Stratigraphy of the Dahomey Basin. Journal of Mining and Geology, 18, 130-137

Philip Kearey, Michael Brooks, Ian Hill (2002), An Introduction to Geophysical Exploration THIRD EDITION

S. A. Amidu, a. I. Olayinka (2006), Environmental Assessment of Sewage Disposal Systems Using 2D Electrical-Resistivity Imaging and Geochemical Analysis: A Case Study from Ibadan, Southwestern Nigeria, Environmental & Engineering Geoscience, Vol. XII, No. 3, pp. 261–272,

Wang, J., Zhang, Z, Z,. Su, Y. M., He, W., He, F (2008)., And Song, H. G. Phytoremediation of Petroleum polluted soil, Petroleum Science, 5(2), 167 -171

Zulfadhli Hasan Adli, Mohd Hafiz Musa, M. N. Khairul Arifin (2010), Electrical Resistivity of Subsurface: Field and Laboratory Assessment, World Academy of Science, Engineering and Technology International Journal of Geological and Environmental Engineering Vol:4, No:9

Zulkarnaini Mat Amin, Norwahidatul Akma Kamal, Norhazimah Husna Shokri and Amalina Yusop (2017), Analysing Petroleum Leakage from Ground Penetrating Radar Signal, B. Pradhan (ed.), Lecture Notes in Civil Engineering 9